The Journal of Supercritical Fluids 181 (2022) 105491

Contents lists available at ScienceDirect

The Journal of Supercritical Fluids

journal homepage: www.elsevier.com/locate/supflu

Multiparameter equation of state for classical and quantum fluids

Roman Tomaschitz

Sechsschimmelgasse 1/21–22, A-1090 Vienna, Austria

HIGHLIGHTS

- An analytic multi-parameter fluid equation of state (EoS) is proposed.
- The critical point conditions and the empirical saturation curve are implemented in the EoS.
- The EoS is non-perturbative and suitable for the high-density regime close to the pressure singularity.
- The EoS is of closed form and applicable in the full temperature range above the melting point.
- The EoS is tested with critical, sub- and supercritical pressure isotherms of water and hydrogen.

GRAPHICAL ABSTRACT

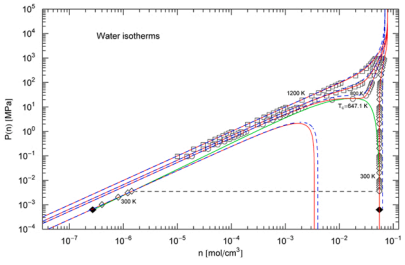

ARTICLE INFO

Keywords:
Non-cubic fluid equation of state (EoS)
Critical, sub- and supercritical isotherms
Vapor–liquid equilibrium and saturation densities
Saturation pressure and coexistence curve
Pressure singularity and limit density
High-pressure EoSs of water and hydrogen

ABSTRACT

A closed-form multi-parameter fluid equation of state (EoS) is proposed and tested with empirical pressure isotherms of water and hydrogen. The EoS is non-algebraic but elementary, applicable in the full temperature range above the melting point, and remains accurate at high pressure. The critical-point conditions (vanishing density-derivatives of pressure) are exactly implemented in the exponential attractive term of the EoS. The singular repulsive term is structured similar to the Carnahan-Starling EoS and depends on five substance-specific parameters, which can be regressed from the critical isotherm. The temperature evolution of the EoS above the critical temperature is regressed from supercritical isotherms. In the subcritical regime above the melting point,

List of symbols and abbreviations[1,2]: EoS, equation of state; P,n,T, pressure, molar density and temperature; $V=1/n$, molar volume; R, universal gas constant; P_c,n_c,T_c,V_c, critical-point constants; $Q(n,T)$, repulsive potential of the EoS, cf. (2.2); $Q_{,n}(n_c,T_c), Q_{,n,n}(n_c,T_c)$, first- and second-order density derivatives of the repulsive potential $Q(n,T)$ at the critical point; Q_0, shortcut for $Q(n_c,T_c)-P_c/R$; b_0, $c_{k=2,3,4}$, β_0, temperature-independent fitting parameters of the repulsive term $Q(n,T)$ of the EoS, b_0 is the limit density where the pressure singularity of the EoS occurs, β_0 is the scaling exponent of pressure at the limit density, and $c_{k=2,3,4}$ are polynomial coefficients of the repulsive term, cf. (2.2); $\rho_{k=2,3,4}(T)$ and $\sigma(T)$, temperature-dependent scale factors of the EoS (2.1), (2.2), referred to as rho and sigma functions on which the EoS linearly depends. The analytic definition of these scale factors is given in (3.4).; A,B, constants defining the exponential in the attractive term of EoS (2.1), calculated as stated in (2.3); $P(n_c,T_c)=P_c$, $P_{,n}(n_c,T_c)=0$, $P_{,n,n}(n_c,T_c)=0$, critical-point conditions, the subscript n preceded by a comma denoting density derivatives; SRK EoS and PR EoS, cubic Soave-Redlich-Kwong equation of state and Peng-Robinson equation of state, cf. Appendix B; χ^2, a least-squares functional to be minimized in the regression, see (3.2), (3.3), (3.5) and also Section 5 for examples of such functionals; dof, degrees of freedom of the χ^2 regression, see the captions to Tables 2, 3 and 5.; $F(n,T)$, $F(V,T)$, Helmholtz free energy, parametrized with molar density or volume and temperature; $F_{,n}$, $F_{,V}$, density and volume derivatives of the Helmholtz free energy; $F_{k=1,2,3,4}(n)$, $F_{\text{attr}}(n)$, integrals occurring in the additive decomposition of the free energy, cf. (4.2), (4.3); $G(V,T)$, Gibbs free energy; $V_1(T)$, $n_1(T)=1/V_1(T)$, molar liquid saturation volume and density, parametrized by temperature, the analytic representation of $V_1(T)$, is stated in (5.1); $V_2(T)$, $n_2(T)=1/V_2(T)$, vapor saturation volume and density, the analytic representation of $V_2(T)$ is stated in (5.3); $P_{\text{sat}}(T)$, saturation pressure, with analytic representation in (5.4); $P_{k=1,2,3,4}(n)$, $P_{\text{attr}}(n)$, components of the additive decomposition of the EoS, cf. (6.1) and (6.3); $f_{k=1,2,3,4}(n)$, $f_{\text{attr}}(n)$, components of the additive decomposition of the Helmholtz free energy, cf. (6.2) and (6.4); $\rho_2(T)=R(\sigma(T),0;T)$, $\rho_3(T)=S(\sigma(T),0;T)$, solutions of the common tangent construction to the free energy, defining the subcritical scale factors $\rho_2(T)$ and $\rho_3(T)$, cf. (6.6).

E-mail address: tom@geminga.org.

https://doi.org/10.1016/j.supflu.2021.105491
Received 20 July 2021; Received in revised form 18 November 2021; Accepted 20 November 2021
Available online 26 November 2021

the temperature-dependent scale factors of the EoS are inferred from the empirical coexistence curve, which is fully implemented in the EoS. The pressure singularity occurs at a limit density that is noticeably higher than predicted by universal cubic EoSs such as the Peng-Robinson EoS. The parameters of the analytic and non-perturbative EoSs of water and hydrogen are derived from high-pressure data sets.

1. Introduction

The aim is to find a practically viable equation of state (EoS) that is sufficiently adaptable to accurately model isotherms and saturation properties of classical and quantum fluids. The proposed closed-form EoS (pressure as a function of density and temperature) fully implements the three conditions $P(n_c,T_c) = P_c, P_{,n} = 0, P_{,nn} = 0$ at the critical point, the subscript n preceded by a comma denoting density derivatives, as well as the empirical coexistence curve. Special attention is given to the ultra-high pressure regime close to the limit density, where the pressure singularity occurs and cubic EoSs [1–8] become increasingly inaccurate. The temperature evolution of the EoS is also given in closed form, in the super- as well as subcritical regimes, without invoking series expansions around the critical temperature.

The EoS is elementary, consisting of a repulsive and attractive term with factorized temperature and density dependence, and is applicable over the full density range below the limit density where the pressure singularity is located. The attractive term is modeled with a density-dependent exponential in contrast to cubic EoSs. Consecutive Maxwell loops [9], which occasionally emerge in multi-parameter EoSs such as the Span−Wagner EoS [10–17], SAFT EoSs [18–27] and Benedict−Webb−Rubin EoS [28,29], do not occur in this case. The subcritical pressure isotherms admit only one loop, i.e. one local maximum followed by one minimum, and the latter can be negative like in cubic EoSs, due to the additive composition, in contrast to multiplicative Dieterici-type EoSs [30,31]. The competing repulsive and attractive terms ensure the existence of negative pressure isotherms in the coexistence region, which are required, for instance, to describe liquid−liquid phase equilibria in multi-component mixtures [32,33]. The subcritical isotherms admit Maxwell loops consistent with the empirical coexistence curve by way of the common tangent construction to the free energy, which is equivalent to the equal-area construction.

The proposed EoS is non-perturbative, designed to stay applicable at ultra-high pressure and density; it does not make use of ab initio intermolecular potentials, which usually necessitate virial expansions; the latter tend to fail at high density and pressure. As there is no atomistic modeling involved, the EoS is applicable to classical and quantum fluids alike, as will be demonstrated with water and hydrogen, using data sets for pressure isotherms and the empirical saturation curve from the NIST Chemistry WebBook [34]; the data for water and hydrogen are based on Refs. [15,29].

In Section 2, the EoS studied in this paper is introduced. A derivation thereof, in particular the implementation of the above mentioned critical point conditions is deferred to Appendix A.

The least-squares regression of critical and supercritical pressure isotherms is discussed in Section 3. In Section 3.1, the temperature-independent parameters of the EoS are inferred from the critical isotherm, using high-pressure data sets of water and hydrogen as examples. In Section 3.2, the regression of supercritical isotherms is explained, and the temperature-dependent analytic scale factors of the EoS in the supercritical regime are obtained in Section 3.3, specifically the scale factors of the EoSs of water and hydrogen.

In Section 4, the free energy is found by integration of the EoS, and the equations defining the saturation curve are derived from the common tangent construction resulting in a convex free energy.

In Section 5, analytic fits to the temperature-dependent empirical liquid and vapor saturation densities and the saturation pressure are performed to obtain closed-form representations of the coexistence curves of water and hydrogen.

In Section 6, we study the EoS in the subcritical regime and implement the coexistence curve into the temperature-dependent scale factors of the EoS, deriving analytic representations of the scale factors valid in the subcritical temperature range above the melting point. In effect, an analytic non-perturbative EoS is obtained, which is consistent with the critical point conditions and the empirical coexistence curve and can be used over the full temperature range above the melting point and over the full density range up to the limit density where the pressure singularity occurs.

Section 7 contains the conclusions. In Appendix A, a derivation of the EoS is given from scratch, as much as possible in analogy to cubic EoSs, starting with the additive van der Waals decomposition; for comparison, universal cubic EoSs are briefly outlined in Appendix B.

2. Closed-form multi-parameter fluid EoS

The analytic closed-form EoS $P(n,T)$ (pressure as a function of density and temperature) studied in this paper is defined as

$$P/R = Q(n,T) - (1-\sigma(T))\,(n/n_c)^2 Q_0 \mathrm{e}^{A(n-n_c)(n-n_c+B)}, \tag{2.1}$$

with repulsive potential

$$Q(n,T) = \frac{1}{(1-n/b_0)^{\beta_0}}\left[Tn + \sum_{k=2}^{4}(1-\rho_k(T))c_k n^k\right] \tag{2.2}$$

A derivation thereof is given in Appendix A; in this section, we just state the basic definitions necessary for the subsequent practical calculations regarding pressure isotherms, free energy and saturation properties, specifically of water and hydrogen. The molar density is denoted by n, and R is the gas constant. The real amplitudes b_0 (positive) and $c_{k=2,3,4}$ and the positive exponent β_0 are fitting parameters independent of temperature. The temperature-dependent scale factors $\rho_{k=2,3,4}(T)$ and $\sigma(T)$ are normalized to $\rho_k(T_c) = \sigma(T_c) = 0$. We will use the shortcuts Q_0, $Q_{,n}$, $Q_{,nn}$ for the constants $Q_0 = Q(n_c,T_c) - P_c/R$ and $Q_{,n}(n_c,T_c)$, $Q_{,nn}(n_c,T_c)$. A subscript comma followed by n denotes a density derivative; accordingly, $Q_{,n}$,$Q_{,nn}$ are the first- and second-order density derivatives of (2.2) taken at the measured critical point (n_c, T_c, P_c), which are explicitly stated in Appendix A, cf. (A.17) and (A.18). The EoS (2.1) linearly depends on the rho and sigma functions $\rho_k(T)$, $\sigma(T)$ yet to be specified, which determine the temperature evolution of the EoS.

The attractive potential in (2.1) factorizes into a temperature-dependent factor $(1-\sigma(T))$ and a density-dependent exponential defined by the constants

$$\begin{aligned} A &:= \frac{1}{n_c^2} + \frac{Q_0 Q_{,nn} - Q_{,n}^2}{2Q_0^2}, \\ B &:= \frac{2n_c Q_0(n_c Q_{,n} - 2Q_0)}{2Q_0^2 - n_c^2 Q_{,n}^2 + n_c^2 Q_0 Q_{,nn}}, \end{aligned} \tag{2.3}$$

derived from the critical point conditions, cf. Appendix A. These constants depend on the critical-point parameters and the fitting parameters of the repulsive term: $A(n_c,T_c,P_c;b_0,\beta_0,c_k)$ and analogously for B. The attractive term in (2.1) scales quadratically $\propto n^2$ in the low-

[1] The ordering of the symbols is according to their first appearance in the text. Listed are quantities used in the main part of the paper, Sections 2–6. Symbols and shortcuts that are only used (and defined) in Appendices A and B are not listed here.

density limit, and the repulsive term (2.2) scales linearly, reproducing the ideal gas law.

The density range of the EoS extends from zero up to the singularity of the repulsive term $Q(n,T)$ at the limit density $n = b_0$. The attractive term in (2.1) is evidently singularity free. The real exponent β_0 of the repulsive term determines the pressure–density scaling close to the pressure singularity. The designation of $Q(n,T)$ as repulsive potential is somewhat arbitrary, since the amplitudes c_k in (2.2) can be negative, so that there are also singular attractive components in the additive $Q(n,T)$. If the exponent in (2.2) is chosen as $\beta_0 = 3$, $Q(n,T)$ becomes structurally similar to the Carnahan-Starling hard-sphere EoS [30,35–38], but we will ultimately settle for the exponent $\beta_0 = 1/2$ in the case of water and hydrogen, cf. Section 3.1.

The EoS defined in (2.1)-(2.3) satisfies the critical-point conditions $P(n_c,T_c) = P_c$, $P_{,n}(n_c,T_c) = 0$, $P_{,nn}(n_c,T_c) = 0$. The derivation of EoS (2.1) in Appendix A is based on these conditions and also on the additive van der Waals ansatz used in cubic equations. In fact, the above EoS is designed in analogy to the cubic Soave-Redlich-Kwong (SRK) and Peng-Robinson (PR) equations, even though the attractive term is an exponential, see the Remark following (A.3).

The pressure P in (2.1) and the critical pressure P_c (the latter occurring in Q_0, cf. after (2.2)) have been rescaled with the gas constant $R = 8.3145\,\mathrm{J/(K\,mol)}$. The pressure unit used is MPa. Thus P/R and $Q(n,T)$ and Q_0 are in units of $\mathrm{K\,mol/cm^3}$. The molar density n is in units of $\mathrm{mol/cm^3}$, and the units of the fitting parameters are $b_0[\mathrm{mol/cm^3}]$, $c_k[\mathrm{K\,(cm^3/mol)}^{k-1}]$. The exponent β_0 is dimensionless. It is possible to make all fitting parameters dimensionless by a rescaling with the critical constants, $\widehat{b}_0 = b_0/n_c$ and $\widehat{c}_k = c_k n_c^{k-1}/T_c$, $k = 2,3,4$, but in contrast to the cubic EoSs in Appendix B, the dimensionless numbers $\widehat{b}_0$, $\widehat{c}_k$ are not universal, cf. Section 3.1.

3. High-pressure isotherms of water and hydrogen

3.1. Least-squares regression of the critical isotherm

In Sections 3 and 4, the EoS (2.1), (2.2) is applied to pressure isotherms of classical and quantum fluids, specifically water and hydrogen, cf. Figs. 1,2. We start with the isotherm passing through the critical point, where the temperature-dependent rho and sigma functions of the EoS vanish, $\sigma(T_c) = \rho_{k=2,3,4}(T_c) = 0$.

At the critical temperature, EoS (2.1), (2.2) reads

$$P/R = \frac{T_c n + c_2 n^2 + c_3 n^3 + c_4 n^4}{(1-n/b_0)^{\beta_0}} - (n/n_c)^2 Q_0 \mathrm{e}^{A(n-n_c)(n-n_c+B)}. \tag{3.1}$$

The amplitude b_0 and the exponent β_0 are positive, and the amplitudes $c_{k=2,3,4}$ are real fitting parameters. The constant $Q_0(n_c,T_c,P_c;b_0,c_k,\beta_0)$ is defined after (2.2). The constants $A(n_c,T_c,P_c;b_0,c_k,\beta_0)$ and $B(n_c,T_c,P_c;b_0,c_k,\beta_0)$ in the exponent of the attractive term are stated in (2.3); their dependence on the fitting parameters stems from the constants Q_0, $Q_{,n}(n_c,T_c;b_0,c_k,\beta_0)$ and $Q_{,nn}(n_c,T_c;b_0,c_k,\beta_0)$ explicitly listed in Appendix A, cf. (A.16)-(A.18).

The EoS (3.1) defines the critical pressure isotherms $P(n;n_c,T_c,P_c;b_0,c_k,\beta_0)$ as a function of density n, the critical point parameters (which are taken as experimental input, cf. Table 1) and the five fitting parameters in the repulsive term (2.2). The conditions $P = P_c$, $P_{,n} = 0$, $P_{,nn} = 0$ are exactly satisfied at the critical point, cf. Appendix A.

The least-squares functional to be minimized in the fit of the critical isotherm reads

$$\chi^2(b_0,c_k,\beta_0) = \sum_{i=1}^{N} \frac{(P(n_i;b_0,c_k,\beta_0) - P_i)^2}{P_i^2}, \tag{3.2}$$

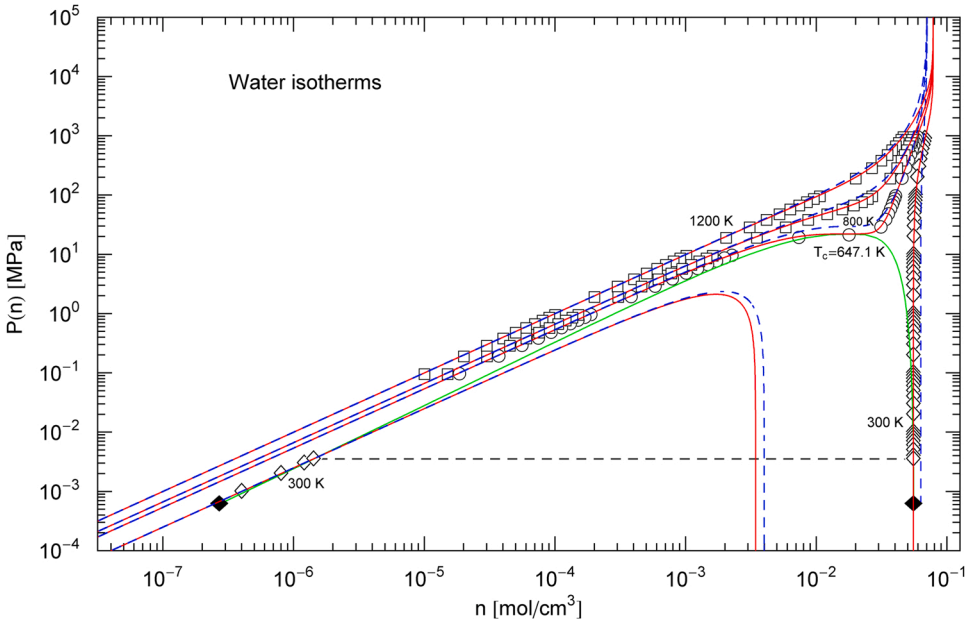

Fig. 1. Water pressure isotherms. Data points from Ref. [34]; squares/circles/diamonds indicate supercritical/ critical/subcritical data points, respectively, at the indicated temperature. The red solid curves show isotherms of EoS (2.1), (2.2). The regression of the critical isotherm (passing through the critical point at T_c) is explained in Section 3.1. The fitting parameters b_0, c_k, β_0 of the critical isotherm, which are temperature-independent and can also be used for super- and subcritical isotherms, are listed in Table 2. Also shown are supercritical isotherms obtained from a four-parameter least-squares fit of the EoS by regressing the rho and sigma scale factors $\rho_{k=2,3,4}(T)$, $\sigma(T)$ at the respective temperature, cf. (3.3) and Table 3. Also depicted are the subcritical 300 K isotherm and the empirical saturation curve (solid green curve), cf. Section 4. The horizontal black dashed line crossing the coexistence region connects the vapor and liquid saturation points on the 300 K isotherm. The black diamonds indicate the end points of the saturation curve. The latter are located on the 273.16 K isotherm (which is not depicted, as it is very close to the 300 K isotherm). The blue dashed curves depict the isotherms of the cubic Peng–Robinson (PR) EoS, cf. Appendix B, with critical point parameters and acentric factor listed in Table 1. The pressure singularity of EoS (2.1), (2.2) occurs at a noticeably higher density (namely b_0 in (2.2) and Table 2) than suggested by universal cubic EoSs (with limit density $\widehat{p}n_c$, cf. after (B.1) and Table 1).

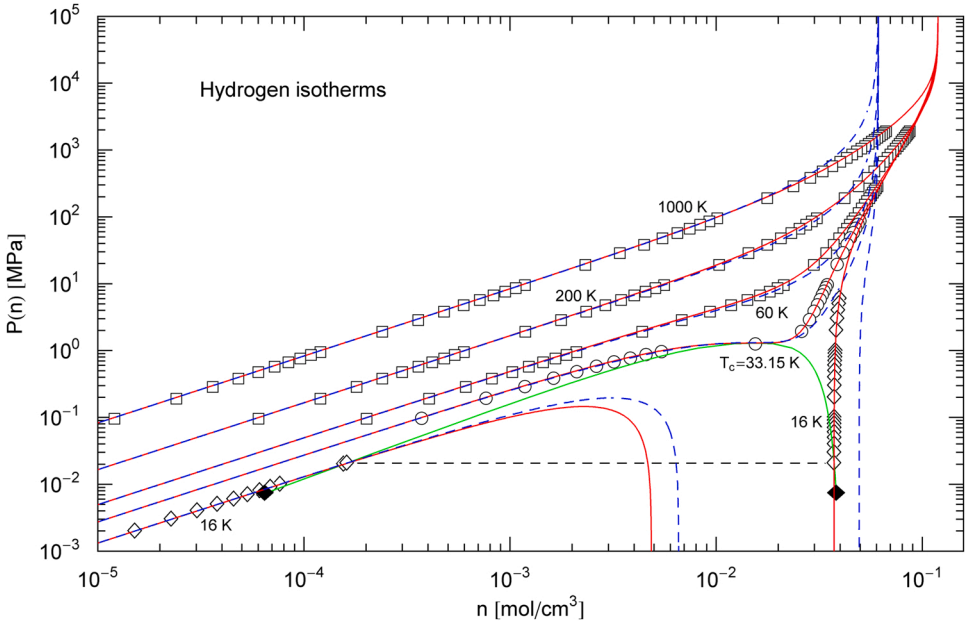

Fig. 2. Hydrogen pressure isotherms. Data points from Ref. [34]; the caption of Fig. 1 applies. The red solid curves are isotherms of EoS (2.1), (2.2). This phenomenological EoS is also applicable to quantum fluids, as there is no atomistic modeling involved requiring quantization. The regression of the critical and supercritical isotherms is explained in Sections 3.1 and 3.2, and subcritical isotherms inferred from the saturation curve (green solid curve) are discussed in Sections 4 and 6. The horizontal dashed line connects vapor and liquid saturation points on the 16 K isotherm, cf. Table 1. The black diamonds are the end points of the saturation curve located on the 13.95 K isotherm (not shown here). For comparison, the blue dashed curves are cubic PR isotherms. The data sets extend beyond the limit density of the PR EoS, cf. after (B.1). The pressure singularity of EoS (2.1), (2.2) is located at the limit density b_0 in Table 2, which is substantially higher than the limit densities of the cubic PR and SRK equations, cf. Appendix B.

Table 1
Critical constants (temperature T_c, molar density n_c, molar volume V_c, and pressure P_c) of water and hydrogen. The critical compressibility factor is $Z_c = P_c/(n_c T_c R)$, see after (B.3). Also listed are the melting temperature T_{melt} and the acentric factor ω of the fluid, the latter used in the cubic PR and SRK EoSs, cf. Appendix B.

	T_c[K]	n_c[mol/cm^3]	V_c[cm^3/mol]	P_c[MPa]	Z_c	T_{melt}[K]	ω
Water	647.10	0.017868	55.967	22.064	0.22951	273.16	0.3443
Hydrogen	33.145	0.015508	64.483	1.2964	0.30334	13.95	− 0.219

where the summation is over density−pressure data points $(n_i, P_i)_{i=1,\dots,N}$ taken at T_c. Evidently, the fitting parameter b_0 defining the singularity of the EoS has to be larger than the highest density n_i in the data set. EoS (3.1) stays well-defined in the admissible density range $0 \le n < b_0$, irrespective of the variation of the fitting parameters, provided that b_0 and β_0 stay positive.

The available density−pressure data sets [34] do not cover densities close to the singularity of the repulsive term of the EoS at $n = b_0$, so that even the approximate location of the pressure singularity is not evident from the data points in Figs. 1 and 2. Therefore, we cannot determine the scaling exponent β_0 at the pressure singularity from the least-squares fit, and we have put $\beta_0 = 1/2$ from the outset; see also the end of this section. Thus, the critical isotherms in Figs. 1 and 2 are obtained by four-parameter $(b_0, c_{k=2,3,4})$ regression.

Figs. 1 and 2 show the critical isotherms (red solid curves) of water and hydrogen, which are based on EoS (3.1) and have been regressed as explained in this section. Data points are from Ref. [34]. The fitting parameters b_0, c_k and the goodness-of-fit parameter χ^2/dof (dof: degrees of freedom) are recorded in Table 2. The isotherms are shown over the full density range, up to the limit density defined by the pressure singularity. The critical isotherm passes through the measured critical point (n_c, T_c, P_c), where the density derivatives of pressure vanish, $P_{,n}(n_c, T_c) = 0$, $P_{,n,n}(n_c, T_c) = 0$. Also depicted are the isotherms of the cubic Peng-Robinson (PR) EoS (blue dashed curves), cf. Appendix B. (The isotherms of the Soave-Redlich-Kwong (SRK) EoS are very similar to the PR EoS.) Also shown in Figs. 1 and 2 are several sub- and supercritical isotherms as well as the coexistence curve (green solid curve), discussed in Sections 3.2 and 4–6.

The isotherms of EoS (3.1) continue smoothly beyond the pressure singularity predicted by the cubic SRK and PR EoSs. Especially in the case of hydrogen, the data sets [34] of the isotherms extend substantially beyond the density limits of the SRK and PR equations, cf. Fig. 2. The density at which the pressure becomes singular is clearly higher than the limit densities of the SRK and PR EoSs. It should also be noted that the location of the pressure singularity, namely the limit density b_0 in (2.16) and Table 2, is correlated with the scaling exponent β_0 at the limit density, which is a positive fitting parameter. As mentioned, because of lack of data points in the last density decade in Figs. 1 and 2, we could not determine β_0 from the least-squares fit of the critical isotherm and have put $\beta_0 = 1/2$. A larger exponent β_0 tends to increase the limit

Table 2
Fitting parameters of the critical pressure isotherms of water and hydrogen in Figs. 1 and 2. The least-squares fits of the critical isotherms are explained in Section 3.1. At the critical temperature, the EoS reads as stated in (3.1), with amplitudes b_0 and $c_{2,3,4}$ as fitting parameters. The exponent β_0 of the repulsive term in (3.1) is also a fitting parameter but has been put to one half for lack of data points defining the density scaling of pressure close to the singularity $n = b_0$, cf. Figs. 1 and 2. The listed parameters b_0, $c_{2,3,4}$ have been rescaled with n_c and T_c to make them dimensionless. Also recorded are the minimum of the least-squares functional χ^2 in (3.2) and the degrees of freedom (dof: number N of data points (n_i, P_i) on the critical isotherm minus number of fitting parameters, four in this case) defining the goodness-of-fit parameter χ^2/dof.

	β_0	b_0/n_c	$c_2 n_c/T_c$	$c_3 n_c^2/T_c$	$c_4 n_c^3/T_c$	χ^2	dof
Water	0.5	4.39101	− 2.12051	0.933256	− 0.0738516	9.43×10^{-4}	34
Hydrogen	0.5	7.69923	− 1.15679	− 0.152727	0.279730	2.12×10^{-4}	24

density b_0. Therefore, the pressure singularity depicted in Figs. 1 and 2 should be regarded as illustrative rather than predictive, since the precise location of the singularity cannot be regressed from the presently available data sets.

3.2. Supercritical isotherms

Given an empirical isotherm at fixed temperature $T = T_j > T_c$, the rho and sigma functions $\rho_{2,3,4}(T_j)$ and $\sigma(T_j)$ of the EoS (2.1), (2.2) at this supercritical temperature can be treated as independent fitting parameters, the only ones of the EoS, since all other parameters have already been determined from the critical isotherm, cf. Section 3.1.

We consider a set of density−pressure data points $(n_i, P_i)_{i=1,\ldots,N}$ defining a supercritical T_j isotherm. The four-parameter χ^2 functional of this isotherm reads

$$\chi^2(\rho_{2,3,4}(T_j), \sigma(T_j)) = \sum_{i=1}^{N} \frac{1}{P_i^2}[P(n_i, T_j; \rho_{2,3,4}(T_j), \sigma(T_j)) - P_i]^2, \tag{3.3}$$

and the parameters $\rho_{2,3,4}(T_j)$ and $\sigma(T_j)$ are found by minimizing this functional. The analytic temperature dependence of the scale factors $\rho_{2,3,4}(T_j)$, $\sigma(T_j)$ above T_c can be found by first regressing $\rho_{2,3,4}(T_j)$, $\sigma(T_j)$ for a sequence of supercritical isotherms $T_{j=1,\ldots,\widehat{N}}$. In this way, four data sets $(T_j, \rho_{2,3,4}(T_j))_{j=1,\ldots,\widehat{N}}$, $(T_j, \sigma(T_j))_{j=1,\ldots,\widehat{N}}$ are generated from which the analytic scale factors $\rho_{2,3,4}(T)$, $\sigma(T)$ can be regressed, cf. Section 3.3.

Several supercritical isotherms of water and hydrogen at selected temperatures T_j are depicted in Figs. 1 and 2 (red solid curves). Each supercritical isotherm was obtained by a four-parameter linear least-squares fit of the EoS (2.1), (2.2) to a data set from Ref. [34], based on χ^2 in (3.3). The temperatures T_j of the selected supercritical isotherms and the regressed parameters $\rho_{2,3,4}(T_j)$, $\sigma(T_j)$ are listed in Table 3, together with the goodness-of-fit parameter χ^2/dof of each T_j isotherm.

The blue dashed curves in Figs. 1 and 2 show the corresponding isotherms (at the same supercritical temperatures T_j) of the cubic PR EoS, cf. Appendix B and Refs. [1–8,39–42]. The isotherms of EoS (2.1), (2.2) extend to higher densities than those of universal cubic EoSs, since the temperature-independent pressure singularity is located at a higher density.

3.3. Scale factors $\rho_k(T)$, $\sigma(T)$ of the EoS in the supercritical regime

To model the analytic temperature dependence of the EoS (2.1), (2.2) above the critical temperature, $T > T_c$, the rho and sigma functions of the EoS need to be specified. To this end, we use the broken power laws, cf. Refs. [43,44],

$$\rho_k(T) = a_k(T/T_c)^{\kappa_k-\lambda_k}(T/T_c - 1)^{\lambda_k},$$
$$\sigma(T) = a_0(T/T_c)^{\kappa_0-\lambda_0}(T/T_c - 1)^{\lambda_0}, \tag{3.4}$$

with $k = 2, 3, 4$. The fitting parameters are the positive amplitudes $a_{k=2,3,4}$ and a_0, the positive exponents $\lambda_{k=2,3,4}$ and λ_0, and the real exponents $\kappa_{k=2,3,4}$ and κ_0. Figs. 3 and 4 show the least-squares fits of the four supercritical scale factors $\rho_k(T; a_k, \kappa_k, \lambda_k)$, $k = 2,3,4$, and $\sigma(T; a_0, \kappa_0, \lambda_0)$ to the data sets $(T_j, \rho_{2,3,4}(T_j))$ and $(T_j, \sigma(T_j))$ of water and hydrogen in Table 3.

The three-parameter least-squares functional to be minimized to obtain the sigma function in (3.4) reads

$$\chi^2(a_0, \kappa_0, \lambda_0) = \sum_{j=1}^{\widehat{N}} \frac{[\sigma(T_j; a_0, \kappa_0, \lambda_0) - \sigma(T_j)]^2}{\sigma^2(T_j)}, \tag{3.5}$$

with data sets $(T_j, \sigma(T_j))$ in Table 3, and analogously for the rho scale factors $\rho_k(T; a_k, \kappa_k, \lambda_k)$ in (3.4). The regressed parameters of the supercritical sigma and rho functions of water and hydrogen (depicted in Figs. 3 and 4) are recorded in Table 4.

4. Helmholtz free energy and coexistence curve

The Helmholtz free energy F is related to pressure by $P = -F_{,V}(V, T)$. (Subscript commas indicate derivatives.) Instead of molar volume, we use molar density $n = 1/V$ as parameter in EoS (2.1), so that $P = F_{,n}n^2$. The molar free energy then reads

$$F(n, T) = \int_{n_c}^{n} \frac{P(n, T)}{n^2} \mathrm{d}n, \tag{4.1}$$

up to a temperature-dependent integration constant independent of density n. The normalization chosen here is $F(n_c, T) = 0$ at the critical density, which suffices for discussing saturation properties.

We split the free energy defined by EoS (2.1), (2.2) into additive components,

$$F(n, T)/R = TF_1(n) + \sum_{k=2}^{4}(1 - \rho_k(T))c_kF_k(n) - (1 - \sigma(T))n_c^{-2}Q_0F_{\text{attr}}(n), \tag{4.2}$$

where

$$F_k(n) := \int_{n_c}^{n} \frac{n^{k-2}\mathrm{d}n}{(1 - n/b_0)^{\beta_0}},$$
$$F_{\text{attr}}(n) := \int_{0}^{n-n_c} \exp(An^2 + ABn)\mathrm{d}n, \tag{4.3}$$

Table 3
Parameters of supercritical pressure isotherms in Figs. 1 and 2. The isotherms are defined by EoS $P(n, T)$ in (2.1), (2.2) at fixed supercritical temperature $T = T_j > T_c$, cf. Section 3.2. The temperature-independent parameters b_0, c_k, β_0 of the EoS are taken from the least-squares fit of the critical isotherm, cf. Table 2. The rho and sigma functions $\rho_{2,3,4}(T_j)$, $\sigma(T_j)$ at temperature T_j are four fitting parameters regressed from the respective empirical T_j isotherm, using data sets from Ref. [34]. Also recorded are the minimum of the least-squares functional χ^2 in (3.3) and the degrees of freedom of each fit. (dof: number N of data points (n_i, P_i) on the respective supercritical T_j isotherm minus four.) At the critical temperature, $\rho_k(T_c) = \sigma(T_c) = 0$, cf. after (2.2).

	T_j[K]	$\rho_2(T_j)$	$\rho_3(T_j)$	$\rho_4(T_j)$	$\sigma(T_j)$	χ^2	dof
Water							
	647.10	0	0	0	0	–	–
	800	0.396993	0.463400	0.881035	0.678376	1.04×10^{-4}	34
	1000	0.614864	0.645551	1.17891	0.920983	7.16×10^{-6}	34
	1200	0.742774	0.695441	1.16563	1.02473	6.55×10^{-6}	33
Hydrogen							
	33.145	0	0	0	0	–	–
	60	0.390456	0.884823	0.168529	0.616792	4.22×10^{-4}	35
	200	1.44592	5.44014	0.712188	1.31870	1.83×10^{-3}	44
	1000	5.85303	9.53558	1.27615	1.96907	6.74×10^{-5}	44

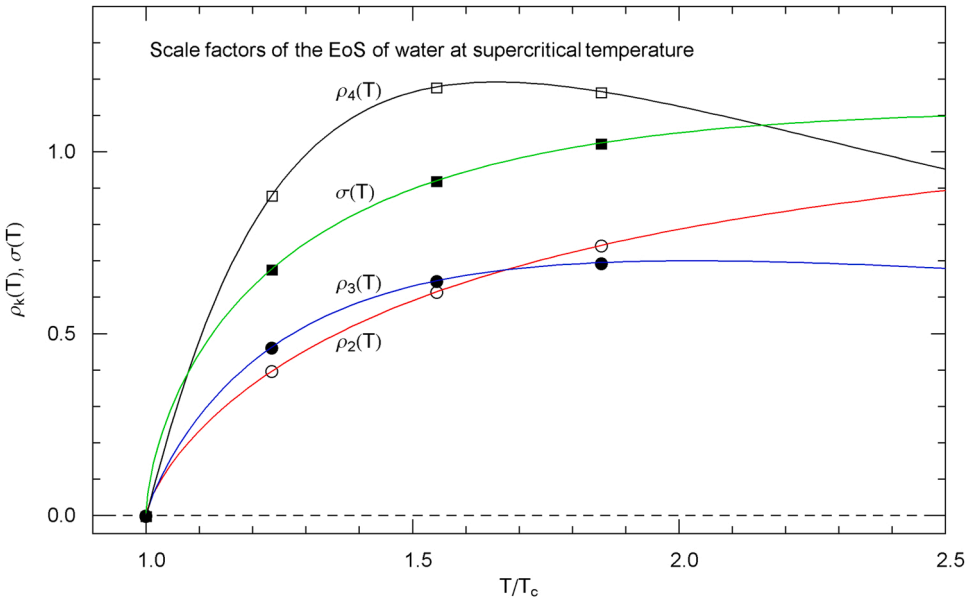

Fig. 3. Scale factors $\rho_{k=2,3,4}(T)$, $\sigma(T)$ of the EoS of water (cf. (2.1), (2.2)) at supercritical temperature $T > T_c$, cf. Sections 3.2 and 3.3. The circles/squares show data points $(T_j, \rho_{2,3,4}(T_j))$, $(T_j, \sigma(T_j))$ from Table 3, at T_c, 800, 1000 and 1200 K. The solid curves depict the regressed supercritical rho and sigma functions of the EoS in (3.4), with fitting parameters recorded in Table 4.

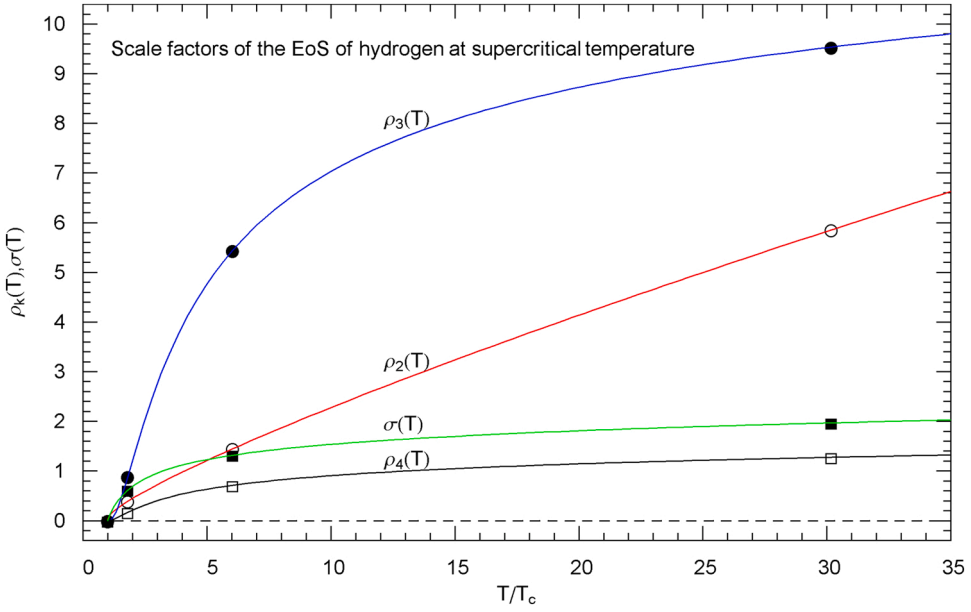

Fig. 4. Scale factors $\rho_{k=2,3,4}(T)$, $\sigma(T)$ of the EoS (2.1), (2.2) of hydrogen at supercritical temperature. The depicted data points $(T_j, \rho_{2,3,4}(T_j))$, $(T_j, \sigma(T_j))$ (circles, squares) are from Table 3, with T_j taking the values T_c, 60, 200 and 1000 K. The least-squares fits of $\rho_{2,3,4}(T)$, $\sigma(T)$ (solid curves) are performed with the rho and sigma functions in (3.4). The χ^2 functional used is stated in (3.5), and the fitting parameters are recorded in Table 4.

Table 4
Fitting parameters of the supercritical rho and sigma functions of the EoSs of water and hydrogen, cf. Section 3.3. Recorded are the parameters of the analytic scale factors $\rho_k(T; a_k, \kappa_k, \lambda_k)$, $k = 2, 3, 4$, and $\sigma(T; a_0, \kappa_0, \lambda_0)$ in (3.4), regressed from supercritical data sets $(T_j, \rho_{2,3,4}(T_j))$ and $(T_j, \sigma(T_j))$ listed in Table 3. The least-squares functional is stated in (3.5). The data points and supercritical scale factors of water and hydrogen are depicted in Figs. 3 and 4, respectively. (Goodness-of-fit parameters are not given in this case, since the curves representing the analytic scale factors in Figs. 3 and 4 pass exactly through the indicated data points.).

	a_2	κ_2	λ_2	a_3	κ_3	λ_3	a_4	κ_4	λ_4	a_0	κ_0	λ_0
Water	1.3081	–0.014613	0.71871	2.2056	–0.81743	0.83804	7.2184	–1.6179	1.0636	1.9880	–0.30724	0.61036
Hydrogen	0.36238	0.82168	0.51374	7.4611	0.098974	2.7252	0.73170	0.18267	1.9613	1.1496	0.16684	0.89770

and $k = 1, 2, 3, 4$. The constants A, B are defined in (2.3), and R in (4.2) is the gas constant. These integrals are either elementary or can be expressed in terms of special functions, but we refrain from doing this here. The free energy (4.2) is evidently linear in the scale factors $\rho_{k=2,3,4}(T)$ and $\sigma(T)$, like EoS (2.1), (2.2). The density n is in units of mol/cm^3, the molar volume $V = 1/n$ in cm^3/mol, the free energy F in J/mol, and 1 MPa = 1 J/cm^3. The volume parametrization of pressure and free energy is obtained by substituting $n = 1/V, n_c = 1/V_c$ in $P(n, T)$ (cf. (2.1)) and $F(n, T)$. (In this case, we simply write $P(V, T)$ and $F(V, T)$; in the following, we will switch back and forth between density and volume parametrization.).

The coexistence curve intersects the subcritical pressure isotherm $P(V, T)$ at the liquid and vapor saturation points $[V_1(T), P(V_1(T), T)]$ and $[V_2(T), P(V_2(T), T)]$, respectively, where $V_1(T) < V_c$ (saturated liquid) and $V_c < V_2(T)$ (saturated vapor), and $T_{\rm melt} < T < T_c$. Here, $T_{\rm melt}$ denotes the melting temperature and $P(V_1(T), T) = P(V_2(T), T)$ is the saturation pressure $P_{\rm sat}(T)$. The (molar) liquid and vapor saturation volumes (denoted by $V_1(T)$ and $V_2(T)$, respectively) coincide at T_c, $V_1(T_c) = V_2(T_c) = V_c$. The molar liquid and vapor saturation densities are $n_1(T) = 1/V_1(T)$ and $n_2(T) = 1/V_2(T)$, respectively, and $n_1(T) > n_c > n_2(T)$. This also gives the temperature parametrization of the coexistence curve in Figs. 1 and 2 (green solid curve); its liquid branch is $[n_1(T), P(n_1(T), T)]$ covering densities above n_c, and the vapor branch below n_c is parametrized by $[n_2(T), P(n_2(T), T)]$, and the temperature range is $T_{\rm melt} < T < T_c$ in either case. The saturation pressure is $P_{\rm sat}(T) = P(n_1(T), T) = P(n_2(T), T)$. Analytic representations of the empirical liquid and vapor saturation volumes and of the saturation pressure of water and hydrogen will be obtained in Section 5.

The common tangent construction (which makes the Helmholtz free energy $F(V, T)$ convex and is equivalent to the equal-area construction) requires that

$$P(V_1(T), T) = P(V_2(T), T),$$
$$G(V_1(T), T) = G(V_2(T), T), \tag{4.4}$$

where $G(V, T) := F(V, T) + P(V, T)V$ is the Gibbs free energy in volume parametrization. The liquid and vapor saturation volumes can be replaced by the corresponding molar saturation densities, by substituting $V_1(T) = 1/n_1(T)$, $V_2(T) = 1/n_2(T)$.

If the subcritical EoS $P(V, T)$, $T_{\rm melt} < T < T_c$, is known, one can calculate $F(V, T)$ as indicated in (4.2) and (4.3) and solve the system (4.4) for the saturation volumes $V_1(T)$ and $V_2(T)$. The saturation pressure is then found as $P_{\rm sat}(T) = P(V_1(T), T)$ and thus the coexistence curve. (The system (4.4) is nonlinear in $V_1(T)$ and $V_2(T)$.).

Conversely, if the saturation volumes $V_1(T)$, $V_2(T)$ are empirically known, one can solve the system (4.4) (which is linear in the scale factors $\rho_{2,3,4}(T)$ and $\sigma(T)$, cf. (2.1), (2.2) and (4.2)) for $\rho_2(T)$ and $\rho_3(T)$, which become linear functions of $\sigma(T)$ and $\rho_4(T)$. In this way, the $\rho_2(T)$ and $\rho_3(T)$ dependence of the subcritical EoS (2.1), (2.2) can be eliminated, and the remaining scale factors $\sigma(T)$ and $\rho_4(T)$ of the EoS can be determined by least-squares fits to subcritical isotherms quite analogous to the regression of the supercritical scale factors in Section 3.2. This is also the way to implement the empirical coexistence curve in the EoS, which will be discussed in greater detail in the next two sections, specifically for the EoSs of water and hydrogen.

5. Analytic representation of the empirical saturation curves of water and hydrogen

5.1. Saturated liquid

To obtain an analytic representation of the liquid saturation volume $V_1(T)$, cf. Section 4, we perform least-squares fits using the shifted broken power-law distribution, cf. Refs. [44–46],

$$V_1(T) = V_c - b_0 T^{\beta_0} \frac{1}{(1 + (T/b_1)^{\beta_1/\eta_1})^{\eta_1}} (1 - (T/T_c)^{\beta_2/\eta_2})^{\eta_2}, \tag{5.1}$$

which is suitable both for classical and quantum fluids. The fit is performed in the subcritical interval $T_{\rm melt} \le T \le T_c$, where $T_{\rm melt}$ is the melting temperature. The parameters in (5.1) are the positive amplitudes b_0 and b_1, the real exponent β_0 and the positive exponents β_1, η_1 and β_2, η_2 of the power-law factors. The χ^2 functional reads

$$\chi^2\,(b_0, \beta_0; b_1, \beta_1, \eta_1; \beta_2, \eta_2) = \sum_{i=1}^{N} \frac{[V_1(T_i; b_0, \beta_0; b_1, \beta_1, \eta_1; \beta_2, \eta_2) - V_{1,i}]^2}{V_{1,i}^2}, \tag{5.2}$$

where $(T_i, V_{1,i})_{i=1,\dots,N}$ are the data points defining the liquid saturation volume [34]. In practice, one uses the shifted data set $(T_i, V_c - V_{1,i})_{i=1,\dots,N}$, and the broken power law $V_c - V_1(T)$, especially when trying to find an initial guess for the fitting parameters, which is obtained by successively fitting the factors of the broken power law, starting at low temperature close to the melting point, cf. Refs. [44,45]. The blue solid curves in Figs. 5 and 6 show the least-squares fits of the liquid saturation volume of water and hydrogen, respectively, based on the analytic representation $V_1(T)$ in (5.1) and data sets from Ref. [34]; the fitting and goodness-of-fit parameters are recorded in Table 5. The liquid saturation density in the interval $T_{\rm melt} \le T \le T_c$ is obtained as the reciprocal saturation volume, $n_1(T) = 1/V_1(T)$, cf. Section 4.

5.2. Saturated vapor

Analogous to the liquid saturation volume in Section 5.1, an analytic representation of the vapor saturation volume $V_2(T)$ is found by means of the shifted broken power law

$$V_2(T) = V_c + (b_0 T)^{\beta_0}\ (1 + (T/b_1)^{\beta_1/\eta_1})^{\eta_1} (1 - (T/T_c)^{\beta_2/\eta_2})^{\eta_2}, \tag{5.3}$$

in the interval $T_{\rm melt} \le T \le T_c$, with positive amplitudes b_0, b_1, real exponent β_0, and positive exponents β_1, η_1 and β_2, η_2. The χ^2 least-squares functional reads as in (5.2), with $V_1(T)$ replaced by $V_2(T)$; the data set for the vapor saturation volume is denoted by $(T_i, V_{2,i})_{i=1,\dots,N}$, cf. Ref. [34]. Conveniently, one uses the shifted data set $(T_i, V_{2,i} - V_c)_{i=1,\dots,N}$ and the multiplicative broken power law $V_2(T) - V_c$ in the χ^2 functional. The least-squares fits of the vapor saturation volume of water and hydrogen are depicted in Figs. 5 and 6, respectively, as red solid curves; the data points shown in the figures are from Ref. [34], and the fitting parameters of the saturated vapor volume $V_2(T)$ in (5.3) are recorded in Table 6. The vapor saturation density is the reciprocal volume, $n_2(T) = 1/V_2(T)$, with the regressed $V_2(T)$ in (5.3).

5.3. Temperature dependence of the saturation pressure

The empirical saturation pressure $P_{\rm sat}(T)$ of water and hydrogen can accurately be modeled with the broken power law

$$P_{\rm sat}(T) = (b_0 T)^{\beta_0} \frac{1}{(1 + (T/b_1)^{\beta_1/\eta_1})^{\eta_1}}, \tag{5.4}$$

in the interval $T_{\rm melt} \le T \le T_c$. The parameters are the positive amplitudes b_0, b_1, the real exponent β_0 and the positive exponents β_1, η_1. The least-squares functional reads

$$\chi^2(b_0, \beta_0; b_1, \beta_1, \eta_1) = \sum_{i=1}^{N} \frac{[P_{\rm sat}(T_i; b_0, \beta_0; b_1, \beta_1, \eta_1) - P_{{\rm sat},i}]^2}{P_{{\rm sat},i}^2}, \tag{5.5}$$

with data points $(T_i, P_{{\rm sat},i})_{i=1,\dots,N}$ from Ref. [34]. The least-squares fits of the saturation pressure (5.4) of water and hydrogen are shown in Figs. 7 and 8, respectively, as red solid curves and the regressed parameters of $P_{\rm sat}(T)$ in (5.4) are recorded in Table 7.

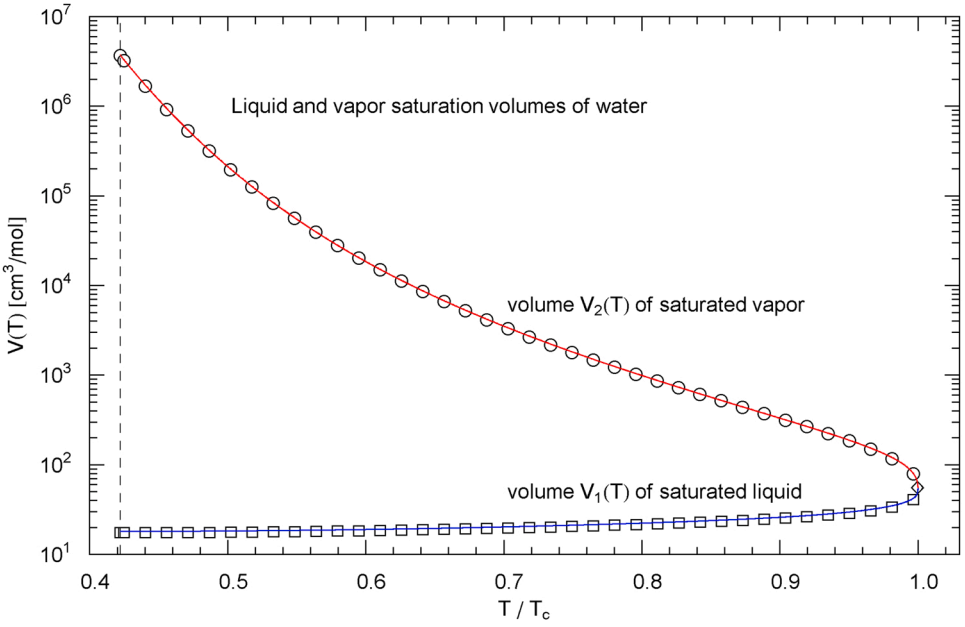

Fig. 5. Molar liquid and vapor saturation volumes of water, cf. Sections 5.1 and 5.2. Data points (squares, circles) from Ref. [34]. The blue solid curve shows the temperature evolution of the liquid saturation volume $V_1(T)$ in (5.1), and the red solid curve depicts the vapor saturation volume $V_2(T)$ in (5.3), in the subcritical temperature interval $T_{\rm melt} \le T \le T_c$. The vertical dashed line indicates the melting temperature. The diamond depicts the critical point (T_c, V_c) where the curves join. The least-squares functional used for the regression is stated in (5.2), and the fitting parameters of $V_1(T)$ and $V_2(T)$ are listed in Tables 5 and 6, respectively.

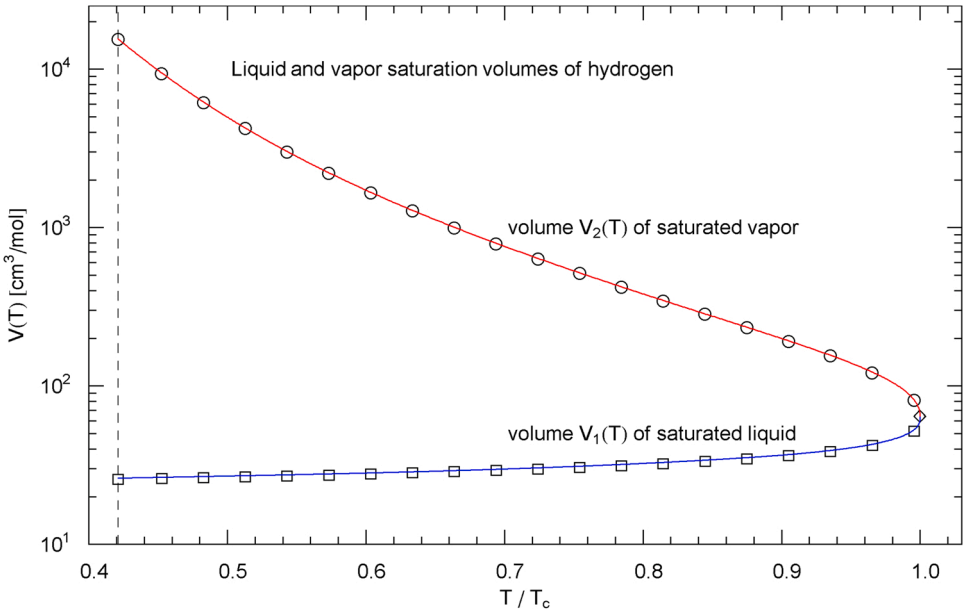

Fig. 6. Liquid and vapor saturation volumes of hydrogen. Data points (squares, circles) from Ref. [34]. The caption of Fig. 5 is applicable. The blue solid curve is the liquid saturation volume $V_1(T)$ in (5.1), and the red solid curve shows the vapor saturation volume $V_2(T)$ of hydrogen in (5.3). The fitting parameters of the saturation volumes are recorded in Tables 5 and 6.

Table 5
Parameters defining the analytic temperature-dependence of the liquid saturation volume $V_1(T)$ of water and hydrogen, cf. Section 5.1. Recorded are the positive amplitudes b_0, b_1, the real exponent β_0 and the positive exponents $\beta_1, \eta_1, \beta_2, \eta_2$ of the shifted and multiply broken power-law distribution $V_1(T)$ in (5.1), obtained by a least-squares fit to data sets from Ref. [34]. The regressed $V_1(T)$ of water and hydrogen is depicted in Figs. 5 and 6, respectively. The listed χ^2 is the minimum of the least-squares functional (5.2); the degrees of freedom (dof: number of data points minus number of fitting parameters) of the χ^2 fits are also recorded.

	$b_0[\mathrm{cm^3 mol^{-1} K^{-\beta_0}}]$	β_0	b_1[K]	β_1	η_1	β_2	η_2	χ^2	dof
Water	35.9264	0.0111419	866.642	6.55514	1.44823	5.44591	0.259458	4.53×10^{-5}	39–7
Hydrogen	50.7635	− 0.106098	31.6649	2.64396	0.406120	7.82273	0.331722	3.23×10^{-5}	20–7

Table 6
Fitting parameters of the vapor saturation volume $V_2(T)$ of water and hydrogen, cf. Section 5.2. The least-squares fits to data sets from Ref. [34] are performed with the shifted and multiply broken power-law density $V_2(T)$ in (5.3). Recorded are the positive amplitudes b_0, b_1, the real exponent β_0 and the positive exponents $\beta_1, \eta_1, \beta_2, \eta_2$ of $V_2(T)$. The least-squares fits of $V_2(T)$ are shown in Figs. 5 and 6. The minimum of the χ^2 functional (assembled analogous to χ^2 in (5.2)) and the degrees of freedom (dof, cf. the caption of Table 5) are also listed.

	$b_0[(\mathrm{cm}^3\ \mathrm{mol}^{-1})^{1/\beta_0}/\mathrm{K}]$	β_0	$b_1[\mathrm{K}]$	β_1	η_1	β_2	η_2	χ^2	dof
Water	1.55617×10^{-3}	− 23.8310	316.497	17.8428	3.68518	9.77111×10^{-7}	0.505820	2.17×10^{-3}	39–7
Hydrogen	2.02351×10^{-2}	− 7.79427	16.1001	3.89609	0.693173	0.321694	0.524407	6.90×10^{-5}	20–7

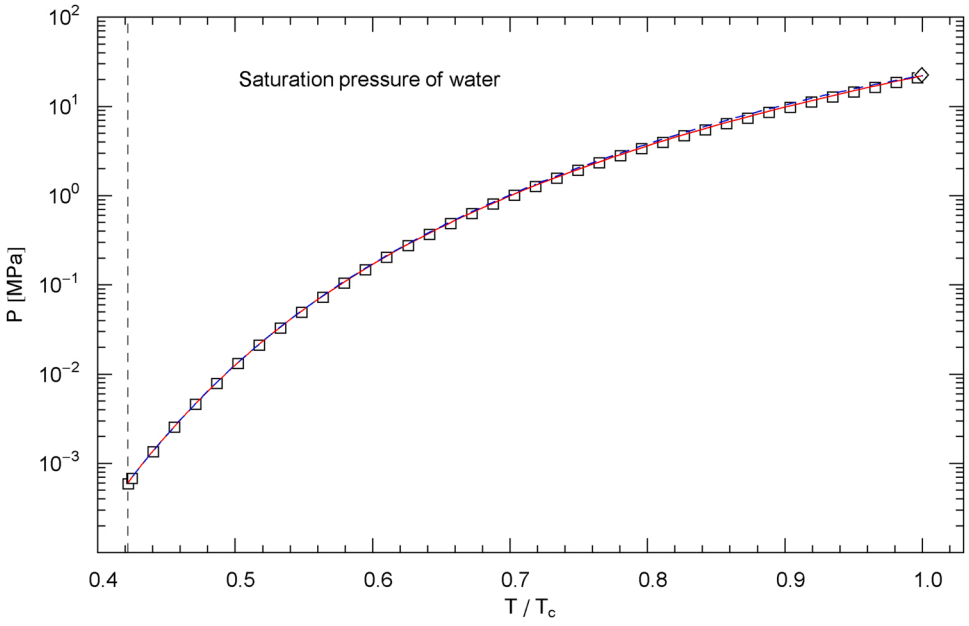

Fig. 7. Saturation pressure of water, cf. Section 5.3. Data points (squares) from Ref. [34]. The red solid curve depicts the regressed saturation pressure $P_{\mathrm{sat}}(T)$, that is the broken power law (5.4), in the interval $T_{\mathrm{melt}} \leq T \leq T_c$, with fitting parameters in Table 7. The least-squares functional used for the regression is stated in (5.5). The diamond indicates the pressure at the critical point (T_c, P_c), cf. Table 1, and the vertical dashed line the melting temperature. The saturation pressure $P(n_1(T), T)$ (blue dashed curve) calculated from the EoS (2.1), (2.2) (with subcritical scale factors in Section 6) and from the liquid saturation density $n_1(T) = 1/V_1(T)$ in Section 5.1 is also indicated as a consistency check, cf. the end of Section 5.3.

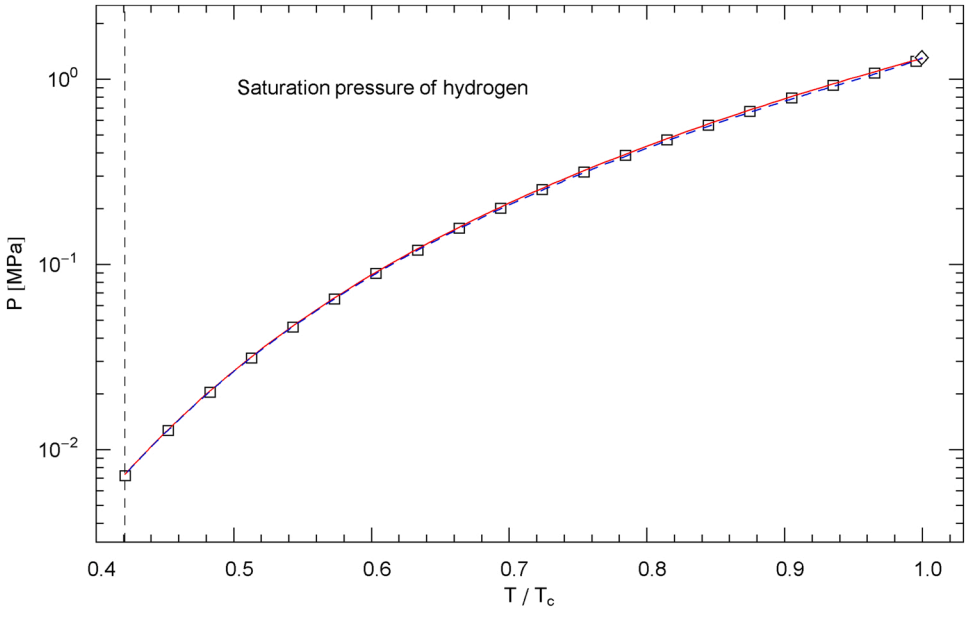

Fig. 8. Saturation pressure of hydrogen, cf. Section 5.3. Data points (squares) from Ref. [34], and the caption of Fig. 7 is applicable. Depicted is the regressed saturation pressure $P_{\mathrm{sat}}(T)$ in (5.4) (red solid curve), in the interval $T_{\mathrm{melt}} \leq T \leq T_c$, with fitting parameters in Table 7. The blue dashed curve depicts the saturation pressure $P(n_1(T), T)$ obtained by substituting the empirical liquid saturation density $n_1(T)$ (cf. Section 5.1) into the EoS (2.1), (2.2) (with subcritical rho and sigma functions in Section 6).

Table 7
Temperature dependence of the saturation pressure of water and hydrogen, cf. Section 5.3. The saturation pressure is modeled with the broken power law $P_{\rm sat}(T)$ in (5.4). The recorded parameters (amplitudes b_0, b_1 and exponents β_0 and β_1, η_1) of $P_{\rm sat}(T)$ are regressed from data sets in Ref. [34]. The least-squares fits of the saturation pressure $P_{\rm sat}(T)$ of water and hydrogen are depicted in Figs. 7 and 8. The minimum of the χ^2 functional (5.5) and the degrees of freedom (dof, cf. the caption of Table 5) are also recorded.

	$b_0[\mathrm{MPa}^{1/\beta_0}/\mathrm{K}]$	β_0	$b_1[\mathrm{K}]$	β_1	η_1	χ^2	dof
Water	3.46434×10^{-3}	32.8121	278.349	27.0900	8.42122	3.11×10^{-4}	39–5
Hydrogen	5.36765×10^{-2}	11.5426	14.1886	7.33898	2.36220	2.32×10^{-5}	20–5

As a consistency check, we note that the empirically regressed $P_{\rm sat}(T)$ in (5.4) should coincide with $P(n_1(T),T)$ and $P(n_2(T),T)$, where $P(n,T)$ is the EoS (2.1), (2.2) with subcritical rho and sigma functions derived in Section 6, see also Section 4. $n_1(T)$ and $n_2(T)$ are the liquid and vapor saturation densities regressed in Sections 5.1 and 5.2. $P(n_1(T),T)$ is identical with $P(n_2(T),T)$, according to the common tangent construction, cf. (4.4), and is depicted in Figs. 7 and 8 as blue dashed curve.

6. Relating the subcritical temperature evolution of the EoS to the saturation curve

The EoS (2.1), (2.2) and the free energy (4.2) are structured as

$$P(n,T)/R = Tp_1(n) + \sum_{k=2}^{4}(1-\rho_k(T))p_k(n) - (1-\sigma(T))p_{\rm attr}(n), \tag{6.1}$$

$$F(n,T)/R = Tf_1(n) + \sum_{k=2}^{4}(1-\rho_k(T))f_k(n) - (1-\sigma(T))f_{\rm attr}(n), \tag{6.2}$$

where

$$p_1(n) := \frac{n}{(1-n/b_0)^{\beta_0}},\ p_k(n) := \frac{c_k n^k}{(1-n/b_0)^{\beta_0}},$$
$$p_{\rm attr}(n) := (n/n_c)^2 Q_0 e^{A(n-n_c)(n-n_c+B)}, \tag{6.3}$$

and, cf. (4.3),

$$f_1(n) := F_1(n),\ f_k(n) := c_k F_k(n),\ f_{\rm attr}(n) := n_c^{-2} Q_0 F_{\rm attr}(n), \tag{6.4}$$

with $k = 2, 3, 4$. One can switch to volume parametrization by substituting $n = 1/V$, $n_c = 1/V_c$ in (6.1)-(6.4), where n denotes the molar density and V the molar volume.

Eq. (4.4) of the common tangent construction can be written as

$$P(n_1(T),T) = P(n_2(T),T),$$
$$F(n_2(T),T) - F(n_1(T),T) = \frac{P(n_1(T),T)}{n_1(T)} - \frac{P(n_2(T),T)}{n_2(T)}, \tag{6.5}$$

where $n_1(T) = 1/V_1(T)$ and $n_2(T) = 1/V_2(T)$ are the analytic liquid and vapor saturation densities in (5.1) and (5.3). In (6.5), we substitute the additive decompositions $P(n,T)$ and $F(n,T)$ stated in (6.1) and (6.2) to obtain two linear equations in four variables $\rho_{2,3,4}(T)$ and $\sigma(T)$. This linear system can be explicitly solved for the scale factors $\rho_2(T)$ and $\rho_3(T)$, which become linear functions of the scale factors $\sigma(T)$ and $\rho_4(T)$,

$$\rho_2(T) = R(\sigma(T),\rho_4(T);T),\ \rho_3(T) = S(\sigma(T),\rho_4(T);T)\,. \tag{6.6}$$

We do not explicitly state these solutions here, since they are clumsy and can easily be obtained with computer algebra software; in Mathematica®, one just applies FullSimplify[Solve[...]] to the linear system (6.5) (with (6.1) and (6.2) inserted) to obtain the solutions (indicated in (6.6)) explicitly.

We substitute solution (6.6) into the EoS (2.1), (2.2), which becomes a linear function of the scale factors $\sigma(T)$ and $\rho_4(T)$. By way of this substitution, the empirical coexistence curve is implemented into the EoS, since the conditions (6.5) of the common tangent construction are then satisfied, irrespective of the choice of the scale factors $\sigma(T)$ and $\rho_4(T)$. These scale factors can be determined by performing least-squares fits to subcritical isotherms, cf. Section 3.2. It suffices to put $\rho_4(T) = 0$ from the outset, and the remaining free parameter $\sigma(T)$ of the EoS can be determined from a one-parameter fit to the respective subcritical T isotherm.

To obtain an analytic representation of $\sigma(T)$, one has to regress $\sigma(T_j)$ from a sequence of subcritical T_j isotherms, $T_{\rm melt} < T_j < T_c$, to obtain a

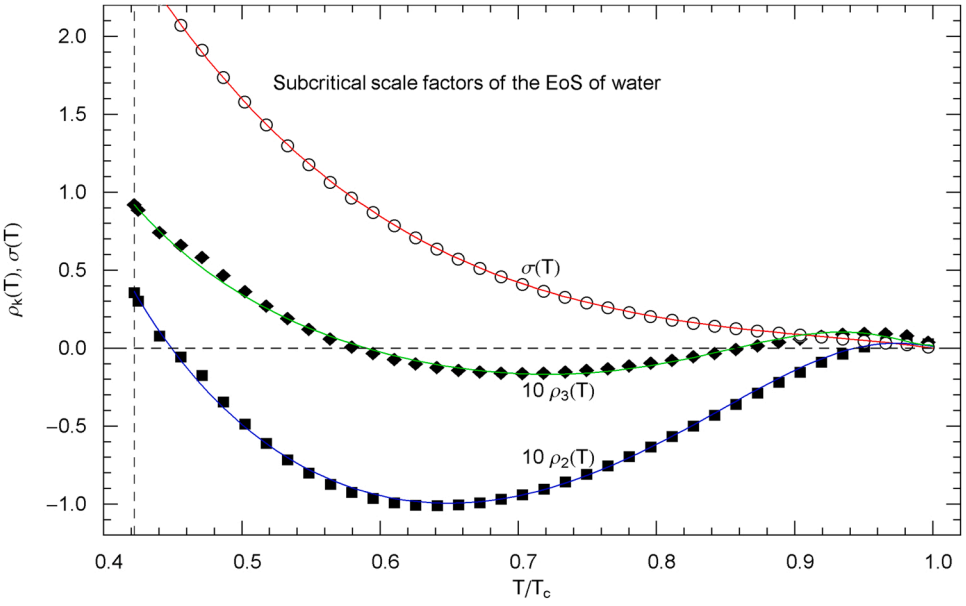

Fig. 9. Subcritical scale factors of the EoS (2.1), (2.2) of water, cf. Section 6. The solid curves show the analytic scale factors $\sigma(T)$ and $\rho_2(T)$, $\rho_3(T)$ of the EoS in the subcritical interval $T_{\rm melt} < T < T_c$. The scale factor $\rho_4(T)$ of EoS (2.1), (2.2) has been put to zero in this interval. The vertical dashed line indicates the melting temperature. The depicted data points were obtained from the empirical coexistence curve and subcritical isotherms, cf. Section 6. (The data points representing the rho functions have been scaled by a factor of 10 for better visualization.) The red solid curve shows the regressed analytic sigma function in (6.7) with parameters in Table 8. The blue and green solid curves depict the analytic rho functions $\rho_2(T)$, $\rho_3(T)$ (cf. (6.6)) obtained from the common tangent construction to the free energy, cf. Sections 4 and 6.

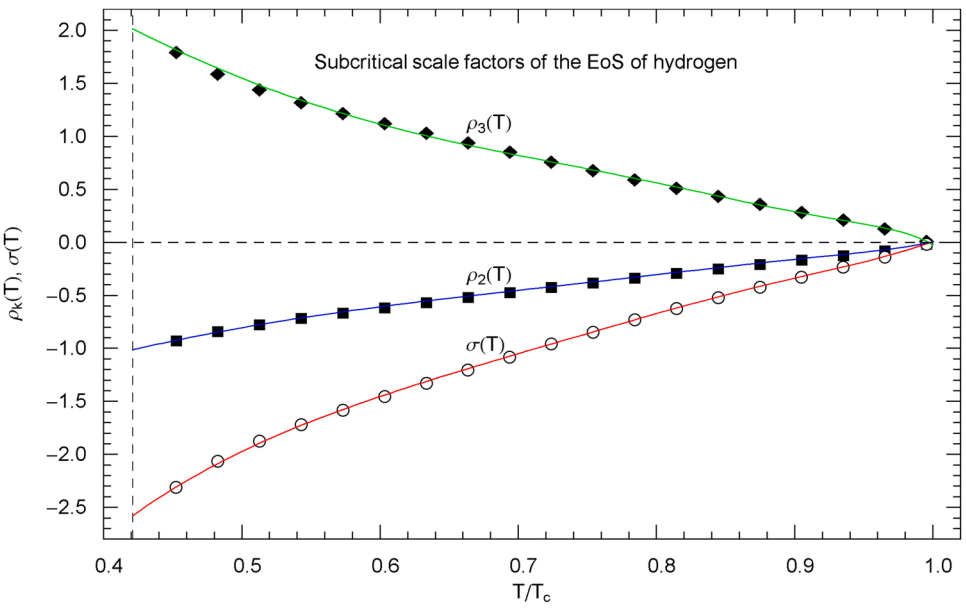

Fig. 10. Subcritical scale factors of the EoS of hydrogen. The caption of Fig. 9 applies. The solid curves show the analytic sigma and rho scale factors $\sigma(T)$, $\rho_2(T)$, $\rho_3(T)$ of EoS (2.1), (2.2). ($\rho_4(T) = 0$ in the subcritical interval $T_{\rm melt} < T < T_c$.) The sigma function is defined by the broken power law (6.7) and fitting parameters in Table 8. The rho functions $\rho_2(T)$, $\rho_3(T)$ are obtained by solving the linear system (6.5) required by the common tangent construction to the free energy, cf. (6.6). The data points are extracted from the empirical coexistence curve and from least-squares fits to subcritical isotherms, cf. Section 6.

data set $(T_j, \sigma(T_j))$. The rho scale factors at the respective temperature are then found via (6.6), $\rho_2(T_j) = R(\sigma(T_j), 0; T_j)$, $\rho_3(T_j) = S(\sigma(T_j), 0; T_j)$ and $\rho_4(T_j) = 0$. Figs. 9 and 10 show the data sets $(T_j, \sigma(T_j))$, $(T_j, \rho_2(T_j))$, $(T_j, \rho_3(T_j))$ for a sequence of subcritical temperatures. (Fig. 9 depicts the subcritical scale factors of the EoS of water and Fig. 10 the scale factors of hydrogen.).

To obtain an analytic representation of the subcritical scale factors $\sigma(T)$ and $\rho_2(T)$, $\rho_3(T)$,

it suffices to regress the sigma function $\sigma(T)$ from the $(T_j, \sigma(T_j))$ data set. This is done by using the broken power-law density, cf. Refs. [44, 45],

$$\sigma(T) = b_0 T^{\beta_0} \frac{1}{(1 + (T/b_1)^{\beta_1/\eta_1})^{\eta_1}} (1 - (T/T_c)^{\beta_2/\eta_2})^{\eta_2} \tag{6.7}$$

in the subcritical interval $T_{\rm melt} < T < T_c$. The fitting parameters are the real amplitude b_0, the real exponent β_0, the positive amplitude b_1 and the positive exponents β_1, η_1 and β_2, η_2, recorded in Table 8 for the sigma functions of water and hydrogen. The χ^2 least-squares functional is assembled like in (5.2) (with V_1 replaced by σ). The regressed sigma function of water and hydrogen is plotted in Figs. 9 and 10 (red solid curve), respectively. The analytic rho functions are obtained by substituting the regressed $\sigma(T)$ into (6.6): $\rho_2(T) = R(\sigma(T), 0; T)$, $\rho_3(T) = S(\sigma(T), 0; T)$, depicted in Figs. 9 and 10 as blue and green solid curves. The subcritical isotherms shown in Figs. 1 and 2 are obtained by using these analytic scale factors (and $\rho_4(T) = 0$) in EoS (2.1), (2.2). The subcritical EoS obtained in this way is in closed form, fully analytic and non-perturbative, and it reproduces the coexistence curve (see Section 5) as well as the empirical subcritical isotherms with high accuracy.

7. Conclusion

The multi-parameter EoS introduced in (2.1), (2.2) and applied to pure water and hydrogen in this paper is elementary and capable of accurately modeling pressure isotherms of classical and quantum fluids, covering the temperature range above the melting point as well as the density range up to the pressure singularity, cf. Figs. 1 and 2. The EoS is analytic and non-atomistic, it does not require microscopic modeling with intermolecular potentials involving series expansions that constrain applications to low pressure and density. The EoS is non-algebraic, yet designed in analogy to cubic EoSs, starting with the additive van-der-Waals decomposition of the EoS into an attractive and repulsive component, cf. Appendix A. The critical-point conditions as well as the empirical saturation curve are fully implemented in the EoS.

The EoS (2.1), (2.2) is parametrized with five temperature-independent parameters, b_0 (limit density at the pressure singularity), β_0 (scaling exponent of pressure at the limit density) and $c_{k=2,3,4}$ (polynomial coefficients of the repulsive term), which can be determined from a least-squares fit of the critical isotherm, cf. Section 3.1. The EoS also depends on three temperature-dependent scale factors $\rho_{k=2,3,4}(T)$ in the repulsive potential and one scale factor $\sigma(T)$ in the attractive potential, which enter linearly in the EoS, cf. (2.1), (2.2). The singular repulsive term (2.2) is itself additive, designed after the Carnahan-Starling EoS, and also contains singular attractive components, cf. Section 2. In the supercritical regime, these rho and sigma functions $\rho_k(T)$, $\sigma(T)$ can be inferred from empirical pressure isotherms at the respective temperature by least-squares regression, cf. Section 3.2. Analytic closed-form expressions of the scale factors of supercritical water and hydrogen were obtained in Section 3.3, cf. Figs. 3 and 4.

Table 8
Parameters of the subcritical sigma function $\sigma(T)$ of water and hydrogen, cf. Section 6. Listed are the real amplitude b_0 and exponent β_0, the positive amplitude b_1 and the positive exponents β_1,η_1, β_2,η_2 of the analytic subcritical scale factor $\sigma(T)$ in (6.7). The least-squares fits of the scale factor $\sigma(T)$ of water and hydrogen are depicted in Figs. 9 and 10, respectively. The minimum of the χ^2 functional (see after (6.7)) and the degrees of freedom (dof, cf. the caption of Table 5) are also recorded.

	b_0[K$^{-\beta_0}$]	β_0	b_1[K]	β_1	η_1	β_2	η_2	χ^2	dof
Water	135.68	− 0.56745	668.91	15.484	6.7331	37.334	1.1022	3.95×10^{-5}	37–7
Hydrogen	− 146.45	− 1.5317	30.298	11.966	1.3516	48.042	1.2727	7.51×10^{-4}	19–7

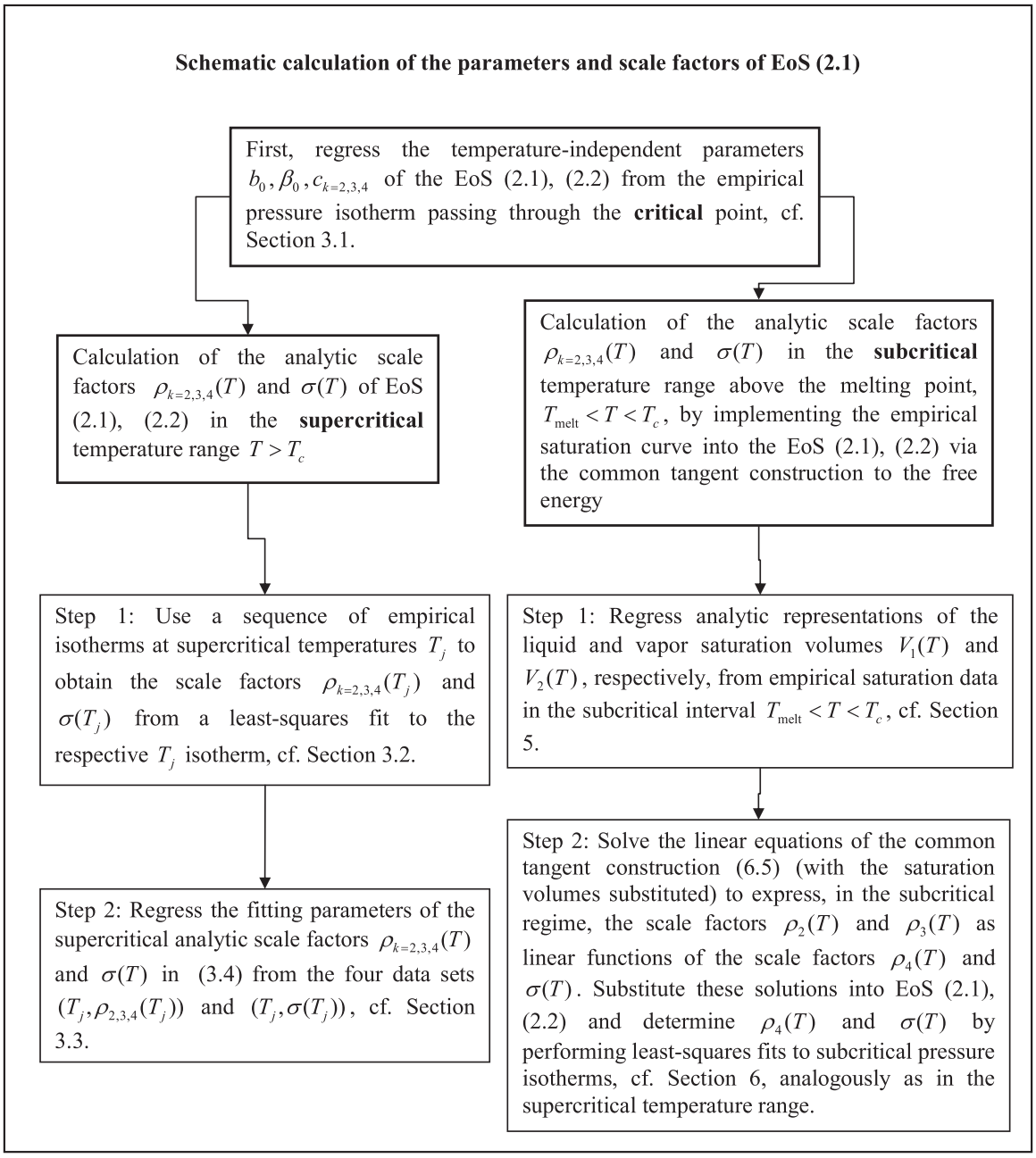

Fig. 11. Flowchart outlining the calculation of the parameters and temperature-dependent scale factors of EoS (2.1), (2.2); see also Section 7 for further discussion. The EoS depends on five temperature-independent parameters, b_0 (limit density at the pressure singularity), β_0 (pressure scaling exponent at the limit density) and $c_{k=2,3,4}$ (polynomial coefficients of the repulsive term (2.2)) as well as on four temperature-dependent scale factors $\rho_{k=2,3,4}(T)$ and $\sigma(T)$, cf. Section 2.

In the subcritical temperature range above the melting point, the temperature-dependent scale factors of the EoS can be calculated from the empirical coexistence curve by way of the common tangent construction to the Helmholtz free energy, cf. Section 4, which amounts to solving a linear system, since the free energy is also linear in the scale factors like the EoS, cf. Section 6. By way of the common tangent construction, the subcritical rho and sigma scale factors become functions of the temperature-dependent liquid and vapor saturation densities, which are empirical input, cf. Section 5. The regression of the temperature-independent parameters b_0, β_0, $c_{k=2,3,4}$ and the temperature-dependent scale factors $\rho_{k=2,3,4}(T)$, $\sigma(T)$ of the EoS (2.1), (2.2) is summarized in the flowchart in Fig. 11.

Critical, super- and subcritical pressure isotherms of water and hydrogen are depicted in Figs. 1 and 2 and compared with the corresponding isotherms of the standard cubic PR EoS. The latter and the very similar cubic SRK EoS are essentially universal equations, depending only on the critical point parameters and the acentric factor, and assume a universal critical compressibility factor, cf. Appendix B. Since this factor is substance dependent in reality, the above mentioned conditions at the critical point can only approximately be satisfied by the PR and SRK equations. More general cubic equations depending on non-universal fitting parameters, involving volume translation for instance [1,2,4,7,8], can exactly reproduce the critical point conditions and also improve the coexistence properties (such as the saturation densities and the saturation pressure), but cannot fully reproduce the empirical saturation curve (depicted in Figs. 1 and 2). The same holds true for SAFT EoSs and generalizations thereof [18–20,22,25], which have specifically been applied to water and hydrogen [21,23,27] and have been tested with empirical coexistence curves.

The limit density of the PR and SRK EoSs, where the pressure becomes singular, universally scales with the critical density, cf. Appendix B. In contrast, the temperature-independent parameters and the temperature-dependent rho and sigma scale factors of EoS (2.1), (2.2) are substance specific and obtained empirically, by least-squares fits to pressure isotherms or, at subcritical temperatures, from the saturation curve, cf. Section 6. The empirical saturation curve is implemented in the EoS without compromising the accuracy of the pressure isotherms, in particular the liquid branches of the subcritical isotherms at high density, which require very accurate modeling because of the extremely steep slopes, cf. Figs. 1 and 2. Since the EoS is not based on the assumption of a specific intermolecular interaction but rather regressed from empirical isotherms and the saturation curve, it is applicable to pure compounds as well as multi-component mixtures. The parameters and scale factors of the EoS are not universal and have to be regressed on a case-by-case basis, for each fluid, to obtain accurate results.

The data sets in Figs. 1 and 2 extend over six decades in pressure, and the isotherms fit accurately even the highest pressure points of the liquid phase, reproducing the experimental subcritical pressure isotherms where the isotherms of the PR and SRK EoSs are way off the mark. In the case of hydrogen, the data sets extend beyond the limit densities suggested by universal cubic EoSs, cf. Fig. 2. Apart from the accuracy of high-pressure isotherms and the empirical coexistence curve reproduced by the EoS, the most important difference between the proposed multi-parameter EoS (2.1), (2.2) and universal cubic EoSs is the pressure singularity occurring at a noticeably higher limit density than the limit densities of the PR and SRK EoSs.

Declaration of Competing Interest

The author declares that he has no known competing financial interests or personal relationships that could have appeared to influence the work reported in this paper.

Appendix A. Setting up a multi-parameter fluid EoS

A.1. Attractive potential of the EoS and implementation of the critical-point conditions

The purpose of this appendix is to give a self-contained derivation of the EoS (2.1), (2.2). The starting point is the additive van der Waals ansatz for a fluid EoS,

$$P = Q(n,T) - (1-\sigma(T))A(n), \tag{A.1}$$

where $Q(n,T)$ and $(1-\sigma(T))A(n)$ are the repulsive and attractive potentials, respectively, to be specified; the (molar) density is denoted by n. The temperature-dependent scale factor $\sigma(T)$ of the attractive term is normalized to zero at the critical temperature, $\sigma(T_c) = 0$. The conditions $P = P_c$, $P_{,n} = 0$, $P_{,n,n} = 0$ at the critical point n_c, T_c, P_c (critical density, temperature and pressure) then read [47],

$$Q - P_c = A,\ Q_{,n} = (Q-P_c)\,\frac{A_{,n}}{A},\ Q_{,n,n} = (Q-P_c)\,\frac{A_{,n,n}}{A}, \tag{A.2}$$

taken at n_c and T_c. The subscript commas followed by n indicate density derivatives. When restoring units, we only need to replace P and P_c by P/R and P_c/R, where R is the gas constant, cf. Section 3.1. The attractive potential in (A.1) is modeled after cubic EoSs (by factorizing the polynomial in the denominator of (B.1), see Appendix B, and replacing the linear factors by real powers),

$$A(n) = \frac{a_1 n^k}{(1+n/b_1)^{\beta_1}(1+n/c_1)^{\eta_1}}, \tag{A.3}$$

with real exponents β_1, η_1, k and amplitudes a_1, b_1, c_1.

Remark: In this section and also in Section A.2, we leave the repulsive term $Q(n,T)$ unspecified. We just note that by specifying $Q(n,T)$ as stated in (2.2) and the attractive term as in (A.3), the resulting EoS is a generalization of the cubic EoSs sketched in Appendix B. In fact, by putting $\beta_1 = \eta_1 = 1$ in (A.3), the denominator becomes a second-order polynomial, and by choosing $\beta_0 = 1$ in (2.2) and dropping the nonlinear terms in the numerator of (2.2), the cubic repulsive term in (B.1) is recovered.

The second and third equation in (A.2) can be written more explicitly as

$$Q_{,n} = Q_0\left(\frac{k}{n} - \frac{\beta_1}{b_1+n} - \frac{\eta_1}{c_1+n}\right) \tag{A.4}$$

and

$$Q_{,n,n} = Q_0\left[\frac{k(k-1)}{n^2} - 2\frac{k}{n}\left(\frac{\beta_1}{b_1+n} + \frac{\eta_1}{c_1+n}\right) + \frac{\beta_1(1+\beta_1)}{(b_1+n)^2} + \frac{\eta_1(1+\eta_1)}{(c_1+n)^2} + \frac{2\beta_1\eta_1}{(b_1+n)(c_1+n)}\right], \tag{A.5}$$

taken at $n = n_c$, $T = T_c$, and we use the shortcut $Q_0 = Q(n_c,T_c) - P_c$, so that $Q_0(n_c,T_c,P_c) = A(n_c)$ in (A.2).

Eqs. (A.4) and (A.5) can explicitly be solved for the exponents β_1 and η_1, admitting a unique solution,

$$\beta_1 = \frac{(b_1+n_c)^2}{(c_1-b_1)Q_0^2}\left[\left(Q_0Q_{,n} - n_cQ_{,n}^2 + n_cQ_0Q_{,n,n}\right) + c_1\left(\frac{k}{n_c^2}Q_0^2 - Q_{,n}^2 + Q_0Q_{,n,n}\right)\right], \tag{A.6}$$

$$\eta_1 = \frac{(c_1+n_c)^2}{(b_1-c_1)Q_0^2}\left[\left(Q_0Q_{,n} - n_cQ_{,n}^2 + n_cQ_0Q_{,n,n}\right) + b_1\left(\frac{k}{n_c^2}Q_0^2 - Q_{,n}^2 + Q_0Q_{,n,n}\right)\right] \tag{A.7}$$

The amplitude a_1 in (A.3) is found by substituting these exponents into $Q_0 = A(n_c)$ (which is the first equation in (A.2)),

$$a_1(n_c,b_1,c_1) = \frac{Q_0}{n_c^k}(1+n_c/b_1)^{\beta_1(n_c,b_1,c_1)}(1+n_c/c_1)^{\eta_1(n_c,b_1,c_1)}. \tag{A.8}$$

The Q_0, $Q_{,n}$, $Q_{,n,n}$ in (A.6)-(A.8) are shortcuts for $Q_0 = Q(n_c,T_c) - P_c$ and the derivatives $Q_{,n}(n_c,T_c)$, $Q_{,n,n}(n_c,T_c)$.

To summarize, the equation of state defined by (A.1) and (A.3) and satisfying the constraints (A.2) reads

$$P = Q(n,T) - \frac{(1-\sigma(T))a_1(n_c,b_1,c_1)n^k}{(1+n/b_1)^{\beta_1(n_c,b_1,c_1)}(1+n/c_1)^{\eta_1(n_c,b_1,c_1)}}, \tag{A.9}$$

with amplitude $a_1(n_c,b_1,c_1)$ and exponents $\beta_1(n_c,b_1,c_1)$ and $\eta_1(n_c,b_1,c_1)$ stated in (A.6)-(A.8). b_1 and c_1 are free fitting parameters. The exponent k is also a free fitting parameter, but we will put $k=2$ from the outset, cf. after (A.15). The scale factor $\sigma(T)$ is unspecified at this point, like the repulsive term $Q(n,T)$ of EoS (A.1), apart from the normalization $\sigma(T_c) = 0$. The exponents β_1, η_1 and amplitude a_1 in the attractive term of EoS (A.9) are determined by the conditions (A.2) and depend on the amplitudes b_1, c_1 as well as on $Q_0 = Q(n_c,T_c) - P_c$ and the density derivatives $Q_{,n}(n_c,T_c)$ and $Q_{,n,n}(n_c,T_c)$ at the critical point. Apart from b_1 and c_1, the fitting parameters of the repulsive term $Q(n,T)$ (yet to be specified) also enter in $a_1(n_c,b_1,c_1)$, $\beta_1(n_c,b_1,c_1)$ and $\eta_1(n_c,b_1,c_1)$ by way of $Q(n_c,T_c)$ and its derivatives $Q_{,n}$ and $Q_{,n,n}$.

A.2. Limit cases of the EoS

We consider a limit case of EoS (A.9), by equating the amplitudes b_1 and c_1 of the attractive term (which are free positive fitting parameters). To this end, we put $c_1 = b_1 + \varepsilon$ and perform the limit $\varepsilon \to 0$. The exponents β_1 and η_1 in (A.6) and (A.7) become singular $\propto 1/\varepsilon$ in this limit, but the attractive term in (A.9) admits a well-defined limit, since

$$\begin{aligned}&(1+n/b_1)^{\beta_1(n_c,b_1,b_1+\varepsilon)}(1+n/(b_1+\varepsilon))^{\eta_1(n_c,b_1,b_1+\varepsilon)}\\ &= \exp\left[-\frac{n}{b_1^2}\frac{\mathrm{sing}(n_c,b_1)}{(1+n/b_1)}\right](1+n/b_1)^{\mathrm{reg}(n_c,b_1)} + \mathrm{O}(\varepsilon),\end{aligned} \tag{A.10}$$

where we use the shortcuts

$$\mathrm{sing}\,(n_c,b_1) := -\frac{(b_1+n_c)^2}{Q_0^2}\left[b_1\left(\frac{k}{n_c^2}Q_0^2 - Q_{,n}^2 + Q_0Q_{,n,n}\right) + Q_0Q_{,n} - n_cQ_{,n}^2 + n_cQ_0Q_{,n,n}\right], \tag{A.11}$$

and

$$\mathrm{reg}\,(n_c,b_1) := \frac{\mathrm{sing}(n_c,b_1)}{b_1+n_c} + \frac{(b_1+n_c)(kQ_0 - n_cQ_{,n})}{n_cQ_0}, \tag{A.12}$$

with $Q_0 = Q(n_c,T_c) - P_c$ and the density derivatives $Q_{,n}(n_c,T_c)$, $Q_{,n,n}(n_c,T_c)$ substituted. The epsilon expansion (A.10) also applies at $n = n_c$, so that the amplitude $a_1(n_c,b_1,b_1+\varepsilon)$ in (A.8) also stays well-defined in the limit $\varepsilon \to 0$.

By performing the $\varepsilon \to 0$ limit, making use of expansion (A.10), the EoS (A.9) simplifies to

$$P = Q(n,T) - (1-\sigma(T))(n/n_c)^kQ_0\exp\left[\frac{n-n_c}{b_1+n}\frac{\mathrm{sing}(n_c,b_1)}{b_1+n_c}\right]\left(\frac{b_1+n_c}{b_1+n}\right)^{\mathrm{reg}(n_c,b_1)}, \tag{A.13}$$

where the functions $\mathrm{sing}(n_c,b_1)$ and $\mathrm{reg}(n_c,b_1)$ are defined in (A.11) and (A.12). b_1 is a free fitting parameter as in EoS (A.9), and the parameter c_1 has been eliminated (by taking the limit $c_1 \to b_1$ as explained above). Like EoS (A.9), this EoS satisfies the conditions (A.2) at the critical point.

EoS (A.13) can be further simplified by performing the limit $b_1 \to \infty$ in the attractive term, which leads to the EoS

$$P = Q(n,T) - (1-\sigma(T))(n/n_c)^kQ_0\mathrm{e}^{A(n-n_c)(n-n_c+B)}, \tag{A.14}$$

where we use the shortcuts

$$A\,(n_c,T_c) = \frac{1}{2}\left(\frac{k}{n_c^2} + \frac{Q_0Q_{,n,n} - Q_{,n}^2}{Q_0^2}\right),\ B(n_c,T_c) = \frac{2n_cQ_0(n_cQ_{,n} - kQ_0)}{kQ_0^2 - n_c^2Q_{,n}^2 + n_c^2Q_0Q_{,n,n}}, \tag{A.15}$$

with $Q_0 = Q(n_c,T_c) - P_c$, $Q_{,n}(n_c,T_c)$ and $Q_{,n,n}(n_c,T_c)$, cf. after (A.8). The exponent in (A.14) is a quadratic polynomial in density n. Thus, by performing the limits $c_1 \to b_1$ and subsequently $b_1 \to \infty$, the free parameters c_1 and b_1 in the attractive term of EoS (A.9) have been eliminated, so that the only fitting parameters in EoS (A.14) are those of the repulsive term $Q(n,T)$ still to be specified. The density-dependent factor $A(n)$ in (A.3) of the attractive term has effectively been turned, by these limits, into a product of n^k with an exponential. The EoS introduced in Section 2 and studied in this paper is obtained by putting $k=2$ in (A.14) and (A.15), so that the attractive term of the EoS scales $\propto n^2$ in the low-density limit.

A.3. Repulsive potential of the EoS

The repulsive term $Q(n,T)$ used in the EoSs (A.9), (A.13) and (A.14) has already been introduced in Section 2. Based on $Q(n,T)$ in (2.2), the

parameter $Q_0 = Q(n_c, T_c) - P_c$ and the derivatives $Q_{,n}(n_c, T_c)$ and $Q_{,n,n}(n_c, T_c)$ at the critical point, which enter in the attractive term of the EoSs (A.9), (A.13), (A.14), can be specified. First,

$$Q_0 = \frac{T_c n_c + c_2 n_c^2 + c_3 n_c^3 + c_4 n_c^4}{(1 - n_c/b_0)^{\beta_0}} - \frac{P_c}{R}, \tag{A.16}$$

where we have also restored the units by rescaling the critical pressure P_c by the gas constant R. (On the left-hand side of the EoSs (A.9), (A.13) and (A.14), we also replace P by P/R.) The density derivatives of the repulsive term $Q(n, T)$ in (2.2) read, at the critical point $n = n_c$, $T = T_c$,

$$Q_{,n} = \frac{1}{(1 - n_c/b_0)^{\beta_0}} \left(T_c + 2c_2 n_c + 3c_3 n_c^2 + 4c_4 n_c^3 + \beta_0 n_c \frac{T_c + c_2 n_c + c_3 n_c^2 + c_4 n_c^3}{b_0 - n_c} \right), \tag{A.17}$$

and

$$Q_{,n,n} = \frac{1}{(1 - n_c/b_0)^{\beta_0}} \left(2c_2 + 6c_3 n_c + 12 c_4 n_c^2 + 2\beta_0 \frac{T_c + 2c_2 n_c + 3c_3 n_c^2 + 4c_4 n_c^3}{b_0 - n_c} \right.$$
$$\left. + \beta_0 (1 + \beta_0) n_c \frac{T_c + c_2 n_c + c_3 n_c^2 + c_4 n_c^3}{(b_0 - n_c)^2} \right) \tag{A.18}$$

These constants, $Q_0(n_c, T_c, P_c)$, $Q_{,n}(n_c, T_c)$ and $Q_{,n,n}(n_c, T_c)$, depend on the critical constants n_c, T_c, P_c (which are taken as empirical input) as well as on the temperature-independent fitting parameters b_0, $c_{k=2,3,4}$, β_0 of the repulsive term (2.2). The EoSs (A.9), (A.13), (A.14) and EoS (2.1) are defined by substituting the repulsive term $Q(n, T)$ stated in (2.2) and the constants Q_0, $Q_{,n}$, $Q_{,n,n}$ listed in (A.16)-(A.18).

Appendix B. Comparison with Soave-Redlich-Kwong and Peng-Robinson EoSs

We briefly outline these equations here, without derivations, since cubic isotherms are used in Figs. 1 and 2 for comparison. These cubic EoSs are of the form, cf. e.g., Refs. [1–8,17,48–50],

$$P/R = \frac{nT}{1 - n/p} - \frac{\alpha(T) a n^2}{1 + n/b + n^2/c}. \tag{B.1}$$

The constants a, b, c, p can be made dimensionless by a rescaling with critical point parameters, $p = \widehat{p} n_c$, $b = \widehat{b} n_c$, $c = \widehat{c} n_c^2$, $a = (T_c/n_c)\widehat{a}$, where the hats indicate universal dimensionless numbers, and R is the gas constant. The Peng-Robinson (PR) equation is defined by $\widehat{p} = 3.9514$, $\widehat{a} = 1.4874$, $\widehat{b} = 1.9757$ and $\widehat{c} = -15.6133$. For the Soave-Redlich-Kwong (SRK) EoS, $\widehat{p} = \widehat{b} = 3.8473$, $\widehat{a} = 1.2824$ and $c = \infty$ (so that the quadratic term in the denominator in (B.1) drops out). The quoted values are approximations of algebraic numbers derived from the roots of a cubic polynomial, cf. e.g., Ref. [47]. The van der Waals equation is defined by $\widehat{p} = 3$, $b = c = \infty$, $\widehat{a} = 9/8$ and $\alpha(T) \equiv 1$.

The alpha function $\alpha(T)$ of the cubic EoS (B.1) is regressed empirically. A frequently used analytic form is $\alpha(T) = (1 + \Omega(\omega)(1 - \sqrt{T/T_c}))^2$, where Ω depends on the acentric factor ω of the fluid [39–41], cf. Table 1. Recent estimates of Ω for the SRK and PR equations are, cf. Ref. [42],

$$\Omega_{\rm SRK}(\omega) = 0.4810 + 1.5963\omega - 0.2963\omega^2 + 0.1223\omega^3, \tag{B.2}$$

$$\Omega_{\rm PR}(\omega) = 0.3919 + 1.4996\omega - 0.2721\omega^2 + 0.1063\omega^3. \tag{B.3}$$

A variety of alternative suggestions for the scale factor $\alpha(T)$ of cubic equations, usually involving truncated power series in $1 - \sqrt{T/T_c}$ or $1 - T/T_c$, can be found in Refs. [51–59].

In Figs. 1 and 2, selected PR pressure isotherms of water and hydrogen are plotted as blue dashed curves and compared with the corresponding isotherms of EoS (2.1), (2.2). The critical compressibility factor $Z_c = P_c/(n_c T_c R)$ of the PR, SRK and van der Waals EoSs is also a universal number, $Z_{c,\rm PR} = 0.30740$, $Z_{c,\rm SRK} = 1/3$ and $Z_{c,\rm vdW} = 3/8$, which is the reason why the empirical critical point (n_c, T_c, P_c) cannot be accurately reproduced by these EoSs. In the case of the EoS (2.1), (2.2), Z_c is not predetermined but calculated from the measured critical constants, cf. Table 1.

References

[1] J.O. Valderrama, The state of the cubic equations of state, Ind. Eng. Chem. Res. 42 (2003) 1603–1618, https://doi.org/10.1021/ie020447b.

[2] A.M. Abudour, S.A. Mohammad, R.L. Robinson Jr., K.A.M. Gasem, Volume-translated Peng–Robinson equation of state for saturated and single-phase liquid densities, Fluid Phase Equil. 335 (2012) 74–87, https://doi.org/10.1016/j.fluid.2012.08.013.

[3] R. Privat, M. Visconte, A. Zazoua-Khames, J.-N. Jaubert, R. Gani, Analysis and prediction of the alpha-function parameters used in cubic equations of state, Chem. Eng. Sci. 126 (2015) 584–603, https://doi.org/10.1016/j.ces.2014.12.040.

[4] J.S. Lopez-Echeverry, S. Reif-Acherman, E. Araujo-Lopez, Peng-Robinson equation of state: 40 years through cubics, Fluid Phase Equil. 447 (2017) 39–71, https://doi.org/10.1016/j.fluid.2017.05.007.

[5] F. Mangold, St. Pilz, S. Bjelić, F. Vogel, Equation of state and thermodynamic properties for mixtures of H_2O, O_2, N_2, and CO_2 from ambient up to 1000 K and 280 MPa, J. Supercrit. Fluids 153 (2019), 104476, https://doi.org/10.1016/j.supflu.2019.02.016.

[6] G.M. Kontogeorgis, R. Privat, J.-N. Jaubert, Taking another look at the van der Waals equation of state– Almost 150 years later, J. Chem. Eng. Data 64 (2019) 4619–4637, https://doi.org/10.1021/acs.jced.9b00264.

[7] X. Chen, H. Li, An improved volume-translated SRK EOS dedicated to more accurate determination of saturated and single-phase liquid densities, in: Fluid Phase Equil., 2020, 112724, https://doi.org/10.1016/j.fluid.2020.112724.

[8] A. Piña-Martinez, R. Privat, S. Lasala, G. Soave, J.-N. Jaubert, Search for the optimal expression of the volumetric dependence of the attractive contribution in cubic equations of state, Fluid Phase Equil. 522 (2020), 112750, https://doi.org/10.1016/j.fluid.2020.112750.

[9] Ø. Wilhelmsen, A. Aasen, G. Skaugen, P. Aursand, A. Austegard, E. Aursand, M. Aa Gjennestad, H. Lund, G. Linga, M. Hammer, Thermodynamic modeling with equations of state: present challenges with established methods, Ind. Eng. Chem. Res. 56 (2017) 3503–3515, https://doi.org/10.1021/acs.iecr.7b00317.

[10] R. Span, W. Wagner, A new equation of state for carbon dioxide covering the fluid region from the triple-point temperature to 1100 K at pressures up to 800 MPa, J. Phys. Chem. Ref. Data 25 (1996) 1509–1596, https://doi.org/10.1063/1.555991.

[11] R. Span, W. Wagner, On the extrapolation behavior of empirical equations of state, Int. J. Thermophys. 18 (1997) 1415–1443, https://doi.org/10.1007/BF02575343.
[12] R. Span, E.W. Lemmon, R.T. Jacobsen, W. Wagner, A reference quality equation of state for nitrogen, Int. J. Thermophys. 19 (1998) 1121–1132, https://doi.org/10.1023/A:1022689625833.
[13] C. Tegeler, R. Span, W. Wagner, A new equation of state for argon covering the fluid region for temperatures from the melting line to 700 K at pressures up to 1000 MPa, J. Phys. Chem. Ref. Data 28 (1999) 779–850, https://doi.org/10.1063/1.556037.
[14] J. Smukala, R. Span, W. Wagner, New equation of state for ethylene covering the fluid region for temperatures from the melting line to 450 K at pressures up to 300 MPa, J. Phys. Chem. Ref. Data 29 (2000) 1053–1121, https://doi.org/10.1063/1.1329318.
[15] W. Wagner, A. Pruß, The IAPWS formulation 1995 for the thermodynamic properties of ordinary water substance for general and scientific use, J. Phys. Chem. Ref. Data 31 (2002) 387–535, https://doi.org/10.1063/1.1461829.
[16] O. Kunz, W. Wagner, The GERG-2008 wide-range equation of state for natural gases and other mixtures: An expansion of GERG-2004, J. Chem. Eng. Data 57 (2012) 3032–3091, https://doi.org/10.1021/je300655b.
[17] E. Rasmussen, S. Yellapantula, M.J. Martin, How equation of state selection impacts accuracy near the critical point: Forced convection supercritical CO_2 flow over a cylinder, J. Supercrit. Fluids 171 (2021), 105141, https://doi.org/10.1016/j.supflu.2020.105141.
[18] E.A. Müller, K.E. Gubbins, Molecular-based equations of state for associating fluids: a review of SAFT and related approaches, Ind. Eng. Chem. Res. 40 (10) (2001) 2193–2211, https://doi.org/10.1021/ie000773w.
[19] R. Privat, R. Gani, J.-N. Jaubert, Are safe results obtained when the PC-SAFT equation of state is applied to ordinary pure chemicals? Fluid Phase Equil. 295 (2010) 76–92, https://doi.org/10.1016/j.fluid.2010.03.041.
[20] I. Polishuk, A. Mulero, The numerical challenges of SAFT EoS models, Rev. Chem. Eng. 27 (2011) 241–261, https://doi.org/10.1515/REVCE.2011.009.
[21] S. Ahmed, N. Ferrando, J.-C. de Hemptinne, J.-P. Simonin, O. Bernard, O. Baudouin, A new PC-SAFT model for pure water, water−hydrocarbons, and water−oxygenates systems and subsequent modeling of VLE, VLLE, and LLE, J. Chem. Eng. Data 61 (2016) 4178–4190, https://doi.org/10.1021/acs.jced.6b00565.
[22] A. Gonzalez Perez, C. Coquelet, P. Paricaud, A. Chapoy, Comparative study of vapour-liquid equilibrium and density modelling of mixtures related to carbon capture and storage with the SRK, PR, PC-SAFT and SAFT-VR Mie equations of state for industrial uses, Fluid Phase Equil. 440 (2017) 19–35, https://doi.org/10.1016/j.fluid.2017.02.018.
[23] A. Köster, M. Thol, J. Vrabec, Molecular models for the hydrogen age: hydrogen, nitrogen, oxygen, argon, and water, J. Chem. Eng. Data 63 (2018) 305–320, https://doi.org/10.1021/acs.jced.7b00706.
[24] R. Ravetti Duran, P. Escudero Falsetti, L. Muhr, R. Privat, D. Barth, Phase equilibrium study of the ternary system $CO_2 + H_2O$ + ethanol at elevated pressure: thermodynamic model selection. Application to supercritical extraction of polar compounds, J. Supercrit. Fluids 138 (2018) 17–28, https://doi.org/10.1016/j.supflu.2018.03.016.
[25] C. Morales-Díaz, A.L. Cabrera, J.C. de la Fuente, A. Mejía, Modelling of solubility of vitamin K3 derivatives in supercritical carbon dioxide using cubic and SAFT equations of state, J. Supercrit. Fluids 167 (2021), 105040, https://doi.org/10.1016/j.supflu.2020.105040.
[26] R. Villablanca-Ahues, P. López-Porfiri, R.I. Canales, J.C. de la Fuente, High-pressure vapor + liquid equilibria for the binary system CO_2 + (E)-2-hexenal, J. Supercrit. Fluids 168 (2021), 105027, https://doi.org/10.1016/j.supflu.2020.105027.
[27] B.D. Marshall, A modified perturbed chain-statistical associating fluid theory equation of state for water which includes an association dependent hard sphere diameter, AIChE J. 67 (2021), e17342, https://doi.org/10.1002/aic.17342.
[28] B.A. Younglove, Thermophysical properties of fluids. I. Argon, ethylene, parahydrogen, nitrogen, nitrogen trifluoride, and oxygen, J. Phys. Chem. Ref. Data 11 (Suppl. 1) (1982) 1–353. ⟨https://srd.nist.gov/JPCRD/jpcrdS1Vol11.pdf⟩.
[29] J.W. Leachman, R.T. Jacobsen, E.W. Lemmon, Fundamental equations of state for parahydrogen, normal hydrogen, and orthohydrogen, J. Phys. Chem. Ref. Data 38 (2009) 721–748, https://doi.org/10.1063/1.3160306.
[30] R.J. Sadus, Equations of state for fluids: the Dieterici approach revisited, J. Chem. Phys. 115 (2001) 1460–1462, https://doi.org/10.1063/1.1380711.
[31] I. Polishuk, R. González, J.H. Vera, H. Segura, Phase behavior of Dieterici fluids, Phys. Chem. Chem. Phys. 6 (2004) 5189–5194, https://doi.org/10.1039/B410886H.
[32] A. Imre, W.A. Van Hook, Liquid–liquid equilibria in polymer solutions at negative pressure, Chem. Soc. Rev. 27 (1998) 117–123, https://doi.org/10.1039/A827117Z.
[33] A. Drozd-Rzoska, S.J. Rzoska, A.R. Imre, Liquid–liquid phase equilibria in nitrobenzene–hexane critical mixture under negative pressure, Phys. Chem. Chem. Phys. 6 (2004) 2291–2294, https://doi.org/10.1039/B315412B.
[34] E.W. Lemmon, M.O. McLinden, D.G. Friend, in NIST Chemistry WebBook, NIST Standard Reference Database Nr. 69, 2021. ⟨https://webbook.nist.gov/chemistry/fluid/⟩.
[35] N.F. Carnahan, K.E. Starling, Intermolecular repulsions and the equation of state for fluids, AIChE J. 18 (1972) 1184–1198, https://doi.org/10.1002/aic.690180615.
[36] F.L. Román, A. Mulero, F. Cuadros, Simple modifications of the van der Waals and Dieterici equations of state: vapour–liquid equilibrium properties, Phys. Chem. Chem. Phys. 6 (2004) 5402–5409, https://doi.org/10.1039/B411612G.
[37] R.F. Checoni, M. Aznar, Comparative study between cubic and non-cubic equations of state using Carnahan-Starling repulsive term: application of temperature-dependent alpha and beta functions, Int. J. Thermodyn. 17 (2014) 21–26, https://doi.org/10.5541/ijot.77015.
[38] H. Liu, Carnahan-Starling type equations of state for stable hard disk and hard sphere fluids, Mol. Phys. 119 (2021), e1886364, https://doi.org/10.1080/00268976.2021.1886364.
[39] W. Zhao, X. Sun, L. Xia, S. Xiang, Research into the polynomial alpha function for the cubic equation of state, Ind. Eng. Chem. Res. 57 (38) (2018) 12602–12623, https://doi.org/10.1021/acs.iecr.8b02549.
[40] F. Yang, Q. Liu, Y. Duan, Z. Yang, On the temperature dependence of the α function in the cubic equation of state, Chem. Eng. Sci. 192 (2018) 565–575, https://doi.org/10.1016/j.ces.2018.08.014.
[41] W. Zhao, L. Xia, X. Sun, S. Xiang, A review of the alpha functions of cubic equations of state, Int. J. Thermophys. 40 (2019) 105, https://doi.org/10.1007/s10765-019-2567-4.
[42] A. Piña-Martinez, R. Privat, J.-N. Jaubert, D.-Y. Peng, Updated versions of the generalized Soave α-function suitable for the Redlich-Kwong and Peng-Robinson equations of state, Fluid Phase Equil. 485 (2019) 264–269, https://doi.org/10.1016/j.fluid.2018.12.007.
[43] R. Tomaschitz, Extension of finite-strain equations of state to ultra-high pressure, Phys. Lett. A 393 (2021), 127185, https://doi.org/10.1016/j.physleta.2021.127185.
[44] R. Tomaschitz, Multiply broken power-law densities as survival functions: An alternative to Pareto and lognormal fits, Physica A 541 (2020), 123188, https://doi.org/10.1016/j.physa.2019.123188.
[45] R. Tomaschitz, Modeling electrical resistivity and particle fluxes with multiply broken power-law distributions, Eur. Phys. J. Plus 136 (2021) 629, https://doi.org/10.1140/epjp/s13360-021-01542-5.
[46] R. Tomaschitz, Thermodynamics of lattice vibrations in non-cubic crystals: the zinc structure revisited, Acta Crystallogr. A77 (2021) 420–432, https://doi.org/10.1107/S2053273321005507.
[47] R. Tomaschitz, Effective Hamiltonians and empirical fluid equations of state, Fluid Phase Equilib. 496 (2019) 80–92, https://doi.org/10.1016/j.fluid.2019.05.014.
[48] R.A. Lamorgese, W. Ambrosini, R. Mauri, Widom line prediction by the Soave–Redlich–Kwong and Peng–Robinson equations of state, J. Supercrit. Fluids 133 (2018) 367–371, https://doi.org/10.1016/j.supflu.2017.07.031.
[49] G. Carissimi, M.G. Montalbán, F.G. Díaz Baños, G. Víllora, High pressure phase equilibria for binary mixtures of CO_2 + 2-pentanol, vinyl butyrate, 2-pentyl butyrate or butyric acid systems, J. Supercrit. Fluids 135 (2018) 69–77, https://doi.org/10.1016/j.supflu.2018.01.003.
[50] A. Valverde, L. Osmieri, F. Recasens, Binary interaction parameters from reacting mixture data. Supercritical biodiesel process with CO_2 as cosolvent, J. Supercrit. Fluids 143 (2019) 107–119, https://doi.org/10.1016/j.supflu.2018.05.023.
[51] A.F. Young, F.L.P. Pessoa, V.R.R. Ahón, Comparison of 20 alpha functions applied in the Peng–Robinson equation of state for vapor pressure estimation, Ind. Eng. Chem. Res. 55 (22) (2016) 6506–6516, https://doi.org/10.1021/acs.iecr.6b00721.
[52] Y. Le Guennec, S. Lasala, R. Privat, J.-N. Jaubert, A consistency test for α-functions of cubic equations of state, Fluid Phase Equil. 427 (2016) 513–538, https://doi.org/10.1016/j.fluid.2016.07.026.
[53] C. Latsky, N.S. Mabena, C.E. Schwarz, High pressure phase behaviour for the CO_2 + n-dodecane + 3,7-dimethyl-1-octanol system, J. Supercrit. Fluids 149 (2019) 138–150, https://doi.org/10.1016/j.supflu.2019.04.002.
[54] C. Latsky, B.J. Daniels, C.E. Schwarz, High pressure phase behaviour of binary systems containing supercritical solvents and uneven acids, J. Supercrit. Fluids 168 (2021), 105075, https://doi.org/10.1016/j.supflu.2020.105075.
[55] C. Lu, Z. Jin, H. Li, Determination of Hildebrand solubility parameter for pure hydrocarbons by incorporating temperature-dependent volume translation into Peng-Robinson equation of state, J. Supercrit. Fluids 164 (2020), 104945, https://doi.org/10.1016/j.supflu.2020.104945.
[56] Z. Chen, D. Yang, Prediction of phase behaviour for n-alkane-CO_2-water systems with consideration of mutual solubility using Peng-Robinson equation of state, J. Supercrit. Fluids 138 (2018) 174–186, https://doi.org/10.1016/j.supflu.2018.03.020.
[57] P. Mahmoodi, M. Sedigh, Soave alpha function at supercritical temperatures, J. Supercrit. Fluids 112 (2016) 22–36, https://doi.org/10.1016/j.supflu.2016.01.004.
[58] P. Mahmoodi, M. Sedigh, Second derivative of alpha functions in cubic equations of state, J. Supercrit. Fluids 120 (2017) 191–206, https://doi.org/10.1016/j.supflu.2016.05.012.
[59] A.M. Palma, A.J. Queimada, J.A.P. Coutinho, Improved prediction of water properties and phase equilibria with a modified Cubic Plus Association equation of state, Ind. Eng. Chem. Res. 56 (51) (2017) 15163–15176, https://doi.org/10.1021/acs.iecr.7b03522.